 Bull. Chem. Soc. Jpn. Vol. 79, No. 12, 1799–1819 (2006)

Award Accounts

The Chemical Society of Japan Award for Creative Work for 2004

Universality and Specificity of Polymer Gels Viewed by Scattering Methods

Mitsuhiro Shibayama

Institute for Solid State Physics, The University of Tokyo, 5-1-5 Kashiwanoha, Kashiwa, Chiba 277-8581

Received March 6, 2006; E-mail: shibayama@issp.u-tokyo.ac.jp

Concentration fluctuations in polymer gels are composed of dynamic thermal fluctuations and frozen inhomogeneities. Particularly, the latter is a characteristic of gels and is due to cross-linking. The frozen inhomogeneities manifest unique properties in polymer gels. Speckle patterns are commonly observed in gels. The time-correlation function of the scattering intensity entails a power-law behavior at the sol–gel transition. The appearance of speckle patterns is related to the nonergodicity of gels, and the power-law behavior corresponds to the self-similarity of clusters at the gelation threshold. In this review, it will be demonstrated that light scattering is one of the most powerful tools for structure characterization of polymer gels. Then, the universality and specificity of polymer gels will be examined for various types of gels, including physical gels, composite gels, and gelators.

1. Introduction

Throughout the history of mankind, gels have been important. For example, gelatin is purified from glue and is used to make jello. "Glue" is extracted from bones, skins, or intestines of animals and is used as adhesives, stickers, food additives, and so on, for thousands of years. Polysaccharides, such as agarose and carrageenan, are also gelling agents and are used for similar purposes. Basically mankind has been utilizing gels since its emergence. Colloid chemistry, which is a major field in chemistry, originated from "glue chemistry" as the word "colloid" itself comes from Latin "colla," which means "glue." Therefore, it is not an exaggeration to state that gels have been closely related to the development of chemistry from its very beginning. In the 20th century, gels went from being "passive" materials to "functional" materials. The evolution of gel science is briefly described in Fig. 1. Ion-exchange resins were commercialized in Germany in 1930s. Soft contact lens, which is made by spin casting of hydroxyethyl methacrylate (HEMA), was invented by Otto Wichterle and co-workers in Czech Republic.[1] In 1952, he succeeded in preparing a cross-linked gel that absorbed up to 40% of water, which was indeed suitable for eye inplants. Then, in 1960, he invented a centrifugal casting device for lens production, which is today called "spin casting." This is how the dream of a remedy for vision defects, first described by Leonaldo da Vinci in 1508, was realized. Theoretical studies on polymer gels began in the 1940's with the pioneering works of Stockmayer[2] and of Flory–Rehner[3] in 1940s. Stockmayer proposed a tree approximation of gel and determined the sol–gel transition point.[2] Flory and Rehner discussed the equilibrium swelling of polymer gels.[3] The textbook on thermodynamics of polymer solutions written by Flory, "Principles of Polymer Chemistry," became a bible for understanding swelling properties of polymer gels as well.[4] In 1970s, highly water-absorbing gels were developed, and with them, the history of gels entered a new era. Furthermore, the discovery of thermosensitive gels in 1980s opened the door for a variety of applications of gels. Among many kinds of thermosensitive polymeric systems, poly(*N*-isopropyl acrylamide) (PNIPA) hydrogels have been most extensively investigated.[5–8]

Polymer gels had long been a subject of polymer chemistry or polymer physical chemistry before Toyoichi Tanaka proposed the collective diffusion theory of polymer gels in 1973.[9] Since then, gel science became a field of physics as well. Stauffer explained the nature of gels from a concept of connectivity, i.e., "percolation."[10–12] Tanaka found a volume phase transition in aged poly(acrlyamide) (PAAm) hydrogel in 1979.[13] He observed a discrete transition in gel size by a slight change of the composition of water/acetone mixture. The volume phase transition is defined as a discrete (or a continuous) transition in volume by a small change of environmental variables, such as temperature, pH, ionic strength, etc.[14,15] Although this concept was proposed by Dusek and Patterson in 1969,[16] this discovery triggered rapid developments in gel science, such as functional materials including, drug delivery systems, actuators, sensors, lab-on-a-chip technology, and tissue engineering.[17,18] The presence of multiphases, in addition to swollen and shrunken phases, was observed by Annaka and Tanaka in 1990s[19] and indicated the significance of "phases in protein" and molecular recognition.

Needless to say, structures of gels have to be well elucidated

Published on the web December 13, 2006; doi:10.1246/bcsj.79.1799

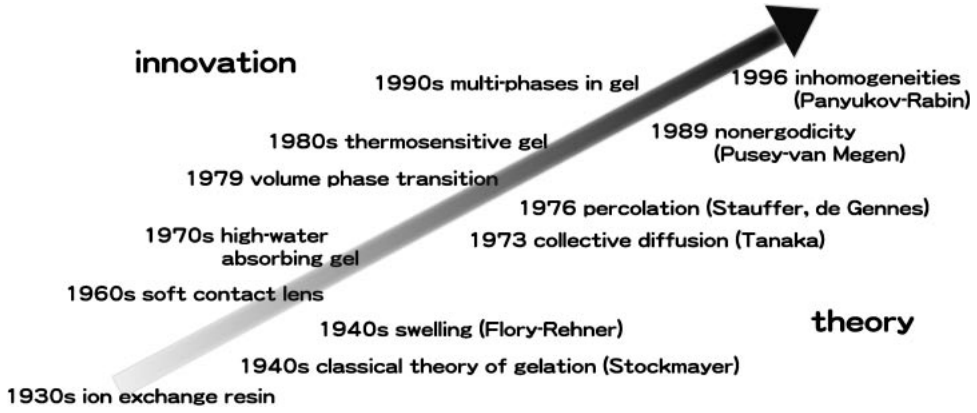

Fig. 1. Overview of the history of gel science.

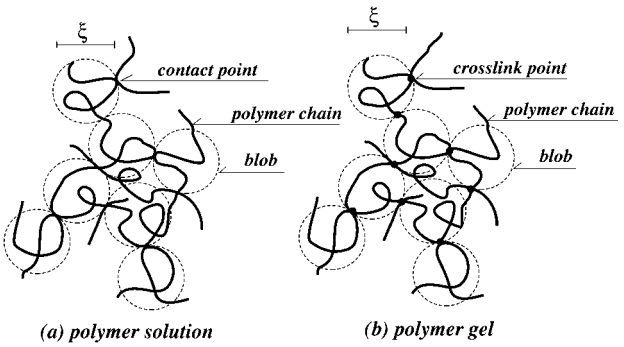

Fig. 2. Comparison of (a) semi-dilute polymer solution and (b) polymer gel. Only the difference is the presence of cross-links in (b).

in order to use gels as functional materials. For example, the optical properties of soft-contact lens, which is a piece of gel swollen in a saline solution, are strongly affected by inhomogeneities and mesoscopic structures in the lens. Shrinking kinetics governs the performance of drug delivery systems, lab-on-a-tips, sensors, actuators, etc. However, structure investigations on polymer gels have been intriguing problems due to complexity of gels, such as cross-linked network, hierarchical structures, and inhomogeneities. Particularly, inhomogeneities, which are rather unique properties of gels, are introduced during cross-linking process. Due to cross-linking, polymer chains in a polymer gel are allowed to travel only a limited excursion in the phase space, i.e., a restricted Brownian motion. This understanding led to the concept of nonergodicity in 1989. In 1996, Panyukov and Rabin proposed a comprehensive theory on the statistical physics of polymer gels.[20] They showed that frozen inhomogeneities in polymer gels can be treated as thermal fluctuations in replica space,[21] and the seemingly interactive calculations of frozen disorder can be performed using the usual methods of equilibrium statistical mechanics.

Figure 2 schematically illustrates the essential difference between a semi-dilute polymer solution and a polymer gel. Here, the cartoons are drawn in order to emphasize that the only difference is the absence/existence of cross-links and that the structure of gels is essentially the same as that of polymer solutions. However, in reality, cross-links play a major role in the unique properties of gels, such as shape sustainability, swelling capability, solvent absorbency, elasticity, molecular recognition, etc. In addition to these properties, which can be observed macroscopically, structural inhomogeneities are not visible in most cases, but strongly influence the physical properties of gels. By focusing on the nature of gels, i.e., cross-linking and inhomogeneities, we carried out a series of works on (1) the decomposition of the concentration fluctuations in gels to the dynamic fluctuations and the static inhomogeneities, (2) the effects of charges on microphase separation in polymer gels, and (3) the development of the time-resolved dynamic light-scattering method which allows determination of gelation threshold.

The objectives of this review are to discuss "the universality and specificity of polymer gels" by investigating the origin of inhomogeneities in polymer gels, proposing methods to characterize inhomogeneities, applying these methods to various types of gels, and relating them with physical properties. Here, an emphasis is placed on the usefulness of the dynamic light-scattering technique and decomposition of concentration fluctuations and classification. Discussions on other interesting topics, such as characterization of inhomogeneites and dynamic concentration fluctuations by scattering methods,[7] gelation mechanism,[22] and charge effects on inhomogeneities,[23] can be found elsewhere.

2. What are Structure Inhomogeneities in Gels?

2.1 Two Types of Concentration Fluctuations and Nonergodicity. Figure 3 illustrates two types of concentration fluctuations in a gel: (a) is the fluctuating component (dynamic thermal fluctuations) that originates from Brownian motion of the solvent and/or the solute, (b) is the frozen concentration inhomogeneities introduced by cross-linking, and (c) is the superposition of (a) and (b). In the case of polymer solutions, only thermal fluctuations exist. In the case of polymer gels, on the other hand, the concentration fluctuations, δc, consist of dynamic fluctuations, δc_{F}, and the frozen (constant) inhomogeneities, δc_{C}, as shown in Fig. 3,

$$\delta c(\mathbf{r}) = \delta c_{\mathrm{F}}(\mathbf{r}) + \delta c_{\mathrm{C}}(\mathbf{r}), \tag{1}$$

where $\mathbf{r}$ is the position vector. Statistically, there are two averages, time average $\langle\ \rangle_{\mathrm{T}}$, and ensemble average $\langle\ \rangle_{\mathrm{E}}$. Since the frozen inhomogeneites do not change with time, a time average of the concentration fluctuations of a gel at a given position is not zero, i.e., $\langle \delta c \rangle_{\mathrm{T}} \neq 0$, while that of the dynamic

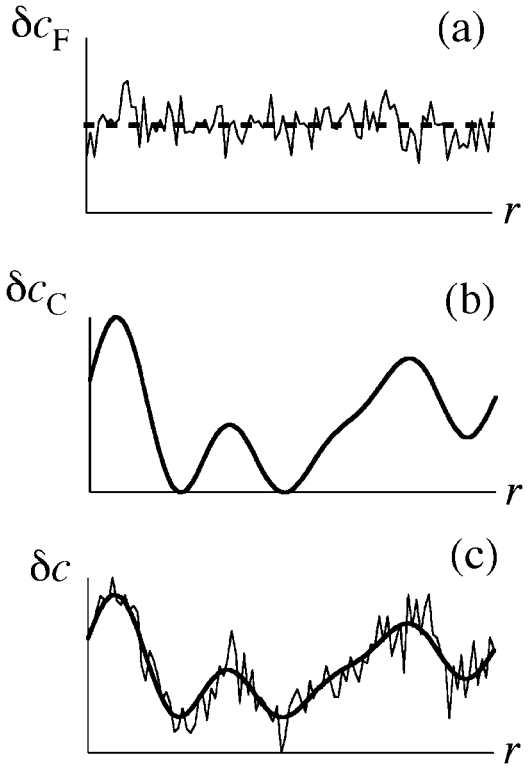

Fig. 3. Two kinds of concentration fluctuations; (a) thermal fluctuations, (b) frozen inhomogeneities, (c) superposition of the two.

fluctuations is zero, i.e., $\langle \delta c_F \rangle_T = 0$. On the other hand, the ensemble average of the frozen inhomogeneities is zero, i.e., $\langle \delta c_C \rangle_E = 0$ by definition. This is why polymer gels have to be treated as nonergodic media.[24] The term "nonergodicity" has been used to describe glasses,[25] and gels.[24,26] It means that the ensemble average and the time average are not equal, i.e.,[27]

$$\langle A \rangle_E \neq \langle A \rangle_T, \tag{2}$$

where A is a variable describing a property of the sample.

In order to characterize these two types of concentration fluctuations, it is more convenient to take Fourier transform of the concentration fluctuations,

$$\delta c(q) = \delta c_F(q) + \delta c_C(q), \tag{3}$$

q is the magnitude of the scattering vector defined by $q = |\mathbf{q}| = (4\pi n/\lambda)\sin(\theta/2)$, n is the refractive index of the scattering medium, and λ is the wavelength of the light in vacuum and θ is the scattering angle. These concentration fluctuations are observed as scattering intensity. Panyukov and Rabin derived the structure factors corresponding to these fluctuations,[20]

$$G(q) \equiv \langle \delta c_F(q) \delta c_F(-q) \rangle_E = \langle \delta c_F(q) \delta c_F(-q) \rangle_T, \tag{4}$$

$$C(q) \equiv \langle \delta c_C(q) \delta c_C(-q) \rangle_E, \tag{5}$$

$$S(q) \equiv \langle \langle \delta c(q) \delta c(-q) \rangle_T \rangle_E = G(q) + C(q). \tag{6}$$

Here, $G(q)$, $C(q)$, and $S(q)$ are the correlators for the dynamic fluctuations, the inhomogeneities, and the structure factor, respectively. Experimentally, small-angle X-ray scattering (SAXS)[28] and small-angle neutron scattering (SANS) have been extensively employed to elucidate the inhomogeneities in polymer gels.[29–34] As a matter of fact, inhomogeneities are one of the most interesting topics in SANS of polymer gels.[7,35] These methods provide information on static scattering, i.e., the ensemble average of concentration. Decomposition of the scattering intensity to two contributions, i.e., δc_F and δc_C, are usually conducted by assuming the dynamic fluctuation of gels being equivalent to those of the corresponding polymer solutions (without cross-links).[7] Dynamic light scattering, on the other hand, allows direct-decomposition of the two contributions as will be discussed in this paper.

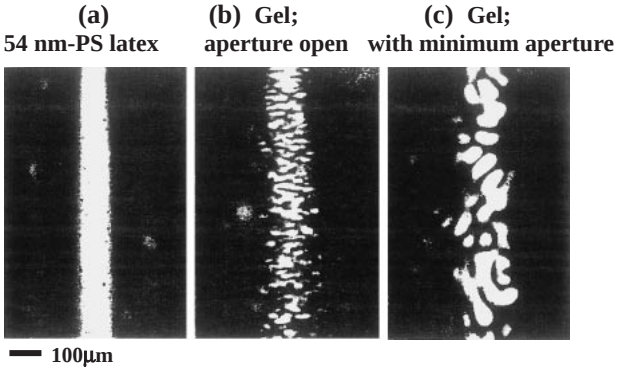

Fig. 4. Traces of laser light beams passing through (a) polystyrene (PS) latex, (b) a gel observed without aperture, and (c) a gel with a minimum aperture. These photographs were taken using an optical microscope [Reproduced with permission from Ph.D. Dissertation, M. Orkisz, MIT, Physics Department, **1994**, Copyright permission: MIT] (Fig. 4 of Chap. 2).

Figure 4 shows optical micrographs of the traces of laser light passing through (a) an ergodic medium (a polystyrene (PS) latex solution) and a nonergodic medium (a polymer gel) (b) with open aperture and (c) with a minimum aperture.[36] In the case of PS latex, a bright band is seen. On the other hand, the trace of laser exhibits "speckles"[37] when it passes through a gel. More interestingly, the spot sizes of the speckles change by changing the aperture size. The larger the aperture is, the finer the speckles are. If one uses a white light from light bulb, such speckles would not appear. These phenomena suggest that the speckle patterns appearing in gels originate from interference of scattered light due to (1) high coherence of laser light and (2) non-vanishing concentration fluctuations in gels, i.e., frozen inhomogeneities.

2.2 Coherency and Coherence Lengths. The size of speckles is determined by the coherence lengths of the optical setup.[37] Figure 5 shows the coherency and the coherence lengths of acoustic wave and electromagnetic waves. Acoustic waves are coherent, resulting in beating. Electromagnetic waves are also coherent. However, light from an electric bulb is not. The coherence of laser light is usually very high due to its monochromatic nature. There are two coherence lengths, the longitudinal, ξ_L, and transverse coherent lengths, ξ_T, defined by[38]

$$\xi_L = \lambda^2/2\Delta\lambda \quad \text{(longitudinal)}. \tag{7}$$

$$\xi_T = z\lambda/2\pi d \quad \text{(transverse)}. \tag{8}$$

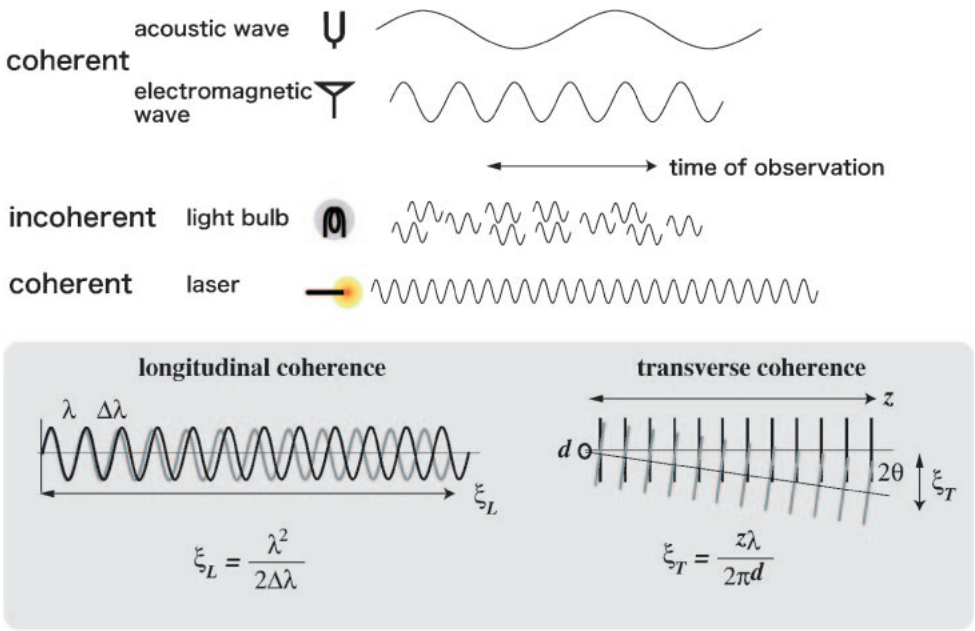

Fig. 5. Coherency and coherence lengths of various waves. ξ_L and ξ_T are the longitudinal and transverse coherence lengths, respectively.

Here, λ and $\Delta\lambda$ are the wavelength and its distribution, respectively, and z is the distance from the aperture with size d to the observation point. The size of speckle patterns is mainly determined by the transverse coherence length, ξ_T, which is a function of the aperture size d. Eq. 8 accounts for the reason why the speckle pattern becomes finer by increasing the aperture size. As a matter of fact, a typical setup for dynamic light scattering (DLS) with a He-Ne laser ($\lambda = 6238$ Å), the sample-to-detector distance of 30 cm, and $d = 1$ mm gives $\xi_T = 32\,\mu$m. This is the same order as the size of speckles observed in a laboratory.

3. Dynamic Light Scattering (DLS)

3.1 DLS as a Basic Tool of Particle Size Determination. DLS is one of the most powerful tools in characterizing concentration fluctuations in polymer solutions and/or colloid dispersions. The observable quantity of DLS is the time correlation function of the scattering intensity, i.e., the so-called second-order correlation function, $g^{(2)}(q,\tau)$,

$$g^{(2)}(\mathbf{q},\tau) = \frac{\langle I(\mathbf{q},0)I(\mathbf{q},\tau)\rangle}{\langle I(\mathbf{q},0)\rangle^2}, \tag{9}$$

where $I(\mathbf{q},\tau)$ is the scattering intensity and τ is the decay time. The angular bracket means averaging. $g^{(2)}(q,\tau)$ is converted to the first-order correlation function, $g^{(1)}(q,\tau)$, via the Siegert relation,[39]

$$g^{(1)}(q,\tau) = \sqrt{g^{(2)}(q,\tau) - 1}. \tag{10}$$

Here, the coherence factor depending on the optical setup is assumed to be unity for simplicity. $g^{(1)}(q,\tau)$ is given by

$$g^{(1)}(\mathbf{q},\tau) = \frac{\langle E(\mathbf{q},t)E^*(\mathbf{q},t+\tau)\rangle}{\langle |E(\mathbf{q},t)|^2\rangle} = \frac{\langle E(\mathbf{q},0)E^*(\mathbf{q},\tau)\rangle}{\langle |E(\mathbf{q},0)|^2\rangle}. \tag{11}$$

Here, $E(\mathbf{q},\tau)$ is the scattering field, and the asterisk means Fourier conjugate. For Brownian objects moving with the translational diffusion coefficient, D_{tr}, $g^{(1)}(q,\tau)$ is obtained by

$$g^{(1)}(q,\tau) = \exp[-D_{tr}q^2\tau]. \tag{12}$$

The size of the diffusing object, i.e., the hydrodynamic radius, R_h, is obtained from $g^{(2)}(q,\tau)$ via Stokes–Einstein equation,

$$R_h = \frac{kT}{6\pi\eta D_{tr}}, \tag{13}$$

where η is the viscosity of the solvent, k is the Boltzmann constant, and T is the absolute temperature.

3.2 Collective Diffusion of Gels and Gel Mode. The above discussion cannot be applied to the dynamics of gels because polymer chains in a gel do not "diffuse" or, more rigorously speaking, do not undergo translational diffusion. The polymer chains in a gel, however, move locally around their average position due to thermal motion, which is called collective diffusion of gels. In 1973, Tanaka, Hocker, and Benedek (THB) realized that a gel has to be treated as a continuum and proposed a theory of collective diffusion of polymer network.[9] This became a standard method to describe the dynamics of gels. This theory predicts that $g^{(2)}(q,\tau)$ is given by a single-exponential function even if cross-links are randomly introduced to a polymer solution.

According to the theory of elasticity,[40] a small deformation of a unit volume of a gel having the mass density, ρ, obeys the following equation,

$$\rho\frac{\partial^2}{\partial t^2}\mathbf{u} = \mu\nabla^2\mathbf{u} + \left(K + \frac{1}{3}\mu\right)\nabla(\nabla\cdot\mathbf{u}) - \zeta\frac{\partial}{\partial t}\mathbf{u}, \tag{14}$$

where $\mathbf{u}(\mathbf{r},t)$ is the displacement vector, which represents the displacement of a point $\mathbf{r}$ on the network from its average position at time t. K and μ are the bulk modulus and the shear modulus, respectively, and ζ is the friction coefficient between the polymer chains and the solvent. This is the fundamental equation to describe not only the dynamics of polymer net-

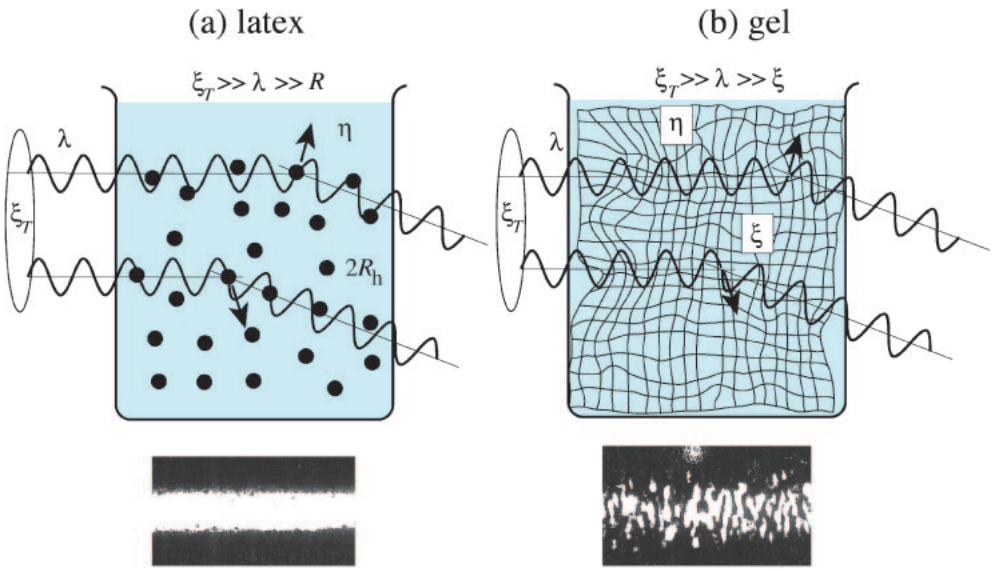

Fig. 6. Comparison of the nature of laser light scattering from (a) a latex (PS spheres in water) and (b) a gel. The solid circles and the mesh indicate PS particles and gel-network, respectively. Both undergo thermal fluctuations due to Brownian motion. The motions of PS particles are totally independent of each other, while those of the network interacted with each other due to chain connectivity. As a result, a speckle pattern appears exclusively in a gel.

works[9] but also the kinetics of gel swelling/shrinking.[41] The left-hand side of Eq. 14 represents the acceleration term, whereas the first two terms of the right-hand side represent the elastic term. The last term of the RHS is the contribution of the friction between the network and solvent molecules. In most cases, however, the acceleration term is negligible compared to the other terms, leading to

$$\zeta \frac{\partial \mathbf{u}}{\partial t} = \left(K + \frac{1}{3}\mu\right)\nabla(\nabla \cdot \mathbf{u}) + \mu \nabla^2 \mathbf{u}. \tag{15}$$

Eq. 15 is further reduced to the well-known diffusion equations given by

$$\frac{\partial u_j}{\partial t} = D \frac{\partial^2 u_j}{\partial x^2}, \tag{16}$$

where D is the collective diffusion coefficient and is given by

$$D = \begin{cases} K + (4/3)\mu/\zeta & \text{(longitudinal)}, \\ \mu/\zeta & \text{(transverse)}, \end{cases} \tag{17}$$

and u_j is the component of the displacement vector along (j = longitudinal) and perpendicular (j = transverse) to the wave vector, respectively.

Assuming that the scattering field at $\mathbf{q}$ and time t, $E(\mathbf{q}, t)$, is proportional to the Fourier transform of the displacement vector, $u(\mathbf{q}, t)$, the time-correlation function for the scattering field, i.e., $g^{(1)}(\mathbf{q}, \tau)$ is obtained as follows,

$$g^{(1)}(q, \tau) = \exp[-D_l q^2 \tau] \quad \text{(polarized light scattering)}, \tag{18}$$

$$g^{(1)}(q, \tau) = \exp[-D_t q^2 \tau] \quad \text{(depolarized light scattering)}, \tag{19}$$

where D_l and D_t are the collective diffusion coefficients along the longitudinal and transverse directions defined by Eq. 17. Note that Eqs. 18 and 19 are the same as the one for the (translational) diffusion of dispersed particles in a dispersant, i.e., Eq. 12. However, the physical meaning of D is different from the translational diffusion coefficient D_{tr} for the case of dispersed particles.

The collective diffusion coefficient is given by[42,43]

$$D = \frac{1}{3N} \int_0^\infty g(\mathbf{r}) \frac{kT}{6\pi\eta r} \mathrm{d}\mathbf{r}, \tag{20}$$

where N is the degree of polymerization of the polymer chains. Since the spatial correlation function for semi-dilute polymer solutions is given by[42]

$$g(r) \approx \frac{\xi}{r} \exp\left(-\frac{r}{\xi}\right), \tag{21}$$

one obtains,

$$D \approx \frac{kT}{6\pi\eta\xi}. \tag{22}$$

Here, the proportional constant has not been determined precisely. It is an issue of future investigation. Figure 6 shows a schematic representation of the difference in the physical meaning of the DLS data obtained for (a) a latex and (b) a gel. In the case of latex solutions, R_h can be observed, while the correlation length, ξ, is observed for gels. Here, ξ can be regarded as the mesh size when the gel is far from the critical region as depicted in Fig. 2. However, ξ is a measure of the distance of concentration correlation. As a matter of fact, ξ diverges at the critical point, while the physical mesh size remains finite.

3.3 Nonergodicity of Gels. The nonuniformity of the scattered light intensity over the sample position, as shown in Fig. 7, was interpreted to be due to the nonergodic nature of the gels. By realizing the inequality in the scattered intensity between ensemble and time averages, Pusey and van Megen proposed the nonergodic medium method for gels.[24] The scattering field for polymer gels contains both a fluctuating component and time-independent component since the chain segments between cross-links are allowed to take a limited

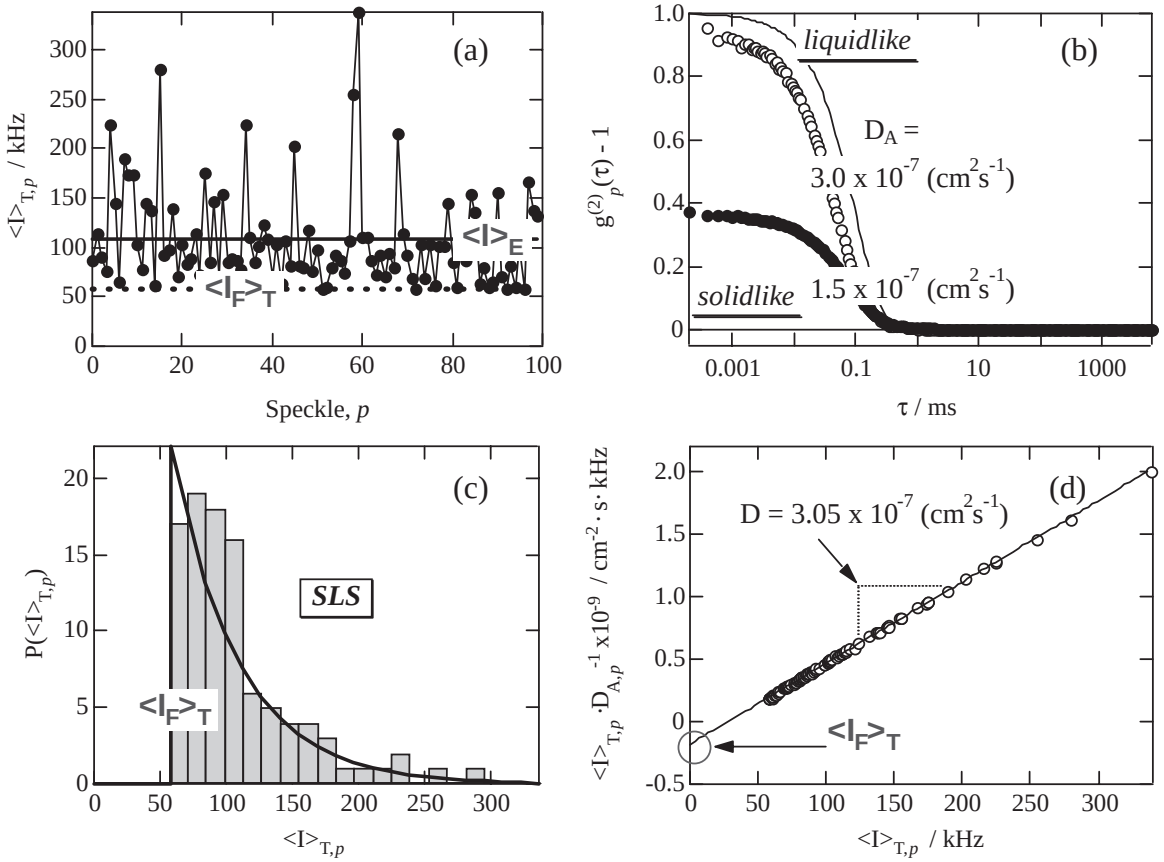

Fig. 7. Characteristic features of a DLS measurement from a gel. (a) A speckle pattern, (b) $g^{(2)}(\tau)$s, (c) an exponential distribution of the scattering intensity, $P(\langle I\rangle_T)$, with a lower cutoff $\langle I_F\rangle_T$, and (d) a linearlized plot for evaluation of the diffusion coefficient, D, and $\langle I_F\rangle_T$.

Brownian motion within a fixed averaged position.[24] Hence, it may be written by,

$$E(t) = E_F(t) + E_C. \tag{23}$$

Here, the subscripts F and C denote the fluctuating and non-fluctuating constant properties, respectively, and have the following properties:

$$\langle E_F(t)E_F{}^*(t)\rangle_E = \langle E_F(t)E_F{}^*(t)\rangle_T = I_F. \tag{24}$$

$$\langle E_{C,p}E_{C,p}{}^*\rangle_E = \langle I_C\rangle_E, \quad \langle E_{C,p}E_{C,p}{}^*\rangle_T = I_{C,p}. \tag{25}$$

Here, the subscript p refers to the sample position. I_F, $I_{C,p}$ are the scattering intensities from the fluctuating and static components, respectively. Note that the latter depends on the sample position at observation. Figure 7a shows a speckle pattern observed for a hydrogel made of PNIPA. The normalized time-correlation function of scattering intensity for a nonergodic system, $g^{(2)}{}_{NE}(q,\tau)$, can be expressed by,[24]

$$g_{NE}{}^{(2)}(q,\tau) \equiv \sum_p \frac{\langle I_p(q,0)I_p(q,\tau)\rangle_T}{\langle I(q,0)\rangle_T^2} = \sum_p \frac{\langle I_F(q,0)I_F(q,\tau)\rangle_T + 2I_{C,p}\langle E_F(q,0)E_F^*(q,\tau)\rangle_T + 2\langle I_F(q)\rangle_T I_{C,p}(q) + I_{C,p}^2(q)}{\langle I(q,0)\rangle_{T,p}^2}. \tag{26}$$

The function $g^{(2)}{}_{NE}(q,\tau)$ defined here contains both decaying and non-decaying components.

$$g_{NE}{}^{(2)}(q,\tau) = 1 + Y^2[\{f_{NE}(q,\tau)\}^2 - \{f_{NE}(q,\infty)\}^2] + 2Y(1-Y)[\{f_{NE}(q,\tau)\} - \{f_{NE}(q,\infty)\}]. \tag{27}$$

Here, $f_{NE}(q,\tau)$ is the time-correlation function for scattering field from a nonergodic system and is given with a diffusion coefficient, D_{NE}, by

$$f_{NE}(q,\tau) = \exp[-D_{NE}q^2\tau]. \tag{28}$$

The variable Y is the ratio of the ensemble to time averages of the scattering intensity, i.e., $Y = \langle I\rangle_E/\langle I\rangle_T$. Hence, Eq. 27 is reduced to Eq. 12 for an ergodic system ($Y = 1$). This concept was also applied to describe hard-sphere colloidal glasses by van Megen et al.[25] However, D_{NE} does not have significant physical meaning because the details of the dynamics in the nonergodic system is smeared out by using an ensemble average. Therefore, the partial heterodyne method, which is discussed in the following section, is more common for discussions of the dynamics of gels.

3.4 Partial Heterodyne Method. Joosten et al. focused on an arbitrary sample position and derived a time average time-correlation function at p,[44]

$$g^{(2)}_{\mathrm{T},p}(q,\tau) \equiv \frac{\langle I(t)I(t+\tau)\rangle_{\mathrm{T},p}}{\langle I(t)\rangle^2_{\mathrm{T},p}} = [X_p g^{(1)}_{\mathrm{F}}(q,\tau)]^2 + 2X_p(1-X_p)g^{(1)}_{\mathrm{F}}(q,\tau) + 1 \quad (29)$$

Here, X_p is the ratio of intensity for the thermal fluctuations to the total intensity, and $g_{\mathrm{F}}{}^{(1)}(q,\tau)$ is the field correlation function of fully fluctuating component, both of which are respectively given by

$$X_p \equiv \frac{\langle I_{\mathrm{F}}\rangle_{\mathrm{T}}}{\langle I\rangle_{\mathrm{T},p}}, \quad (30)$$

$$g^{(1)}_{\mathrm{F}}(q,\tau) = \frac{\langle E_{\mathrm{F}}(q,0)E_{\mathrm{F}}{}^*(q,\tau)\rangle_{\mathrm{E}}}{\langle I_{\mathrm{F}}(q,0)\rangle_{\mathrm{E}}} = \frac{\langle E_{\mathrm{F}}(q,0)E_{\mathrm{F}}{}^*(q,\tau)\rangle_{\mathrm{T}}}{\langle I_{\mathrm{F}}(q,0)\rangle_{\mathrm{T}}}. \quad (31)$$

Note that $g^{(2)}_{\mathrm{F}}(q,\tau)$ in Eq. 29 is dependent on p (Cf. Eq. 20). Figure 7b shows $g^{(2)}_{\mathrm{F}}(q,\tau)$s observed at two different sample positions. The open circles correspond to the correlation function obtained at a low-intensity speckle, while the solid circles to a high-intensity speckle in Fig. 7a. The initial amplitude of $g^{(2)}_{\mathrm{T},p}(q,\tau)$, σ^2_{I} depends on X_p as follows:

$$\sigma^2_{\mathrm{I},p} \equiv g^{(2)}_{\mathrm{T},p}(0) - 1 = X_p(2-X_p). \quad (32)$$

σ^2_{I} is less than unity and sample-position dependent for non-ergodic systems due to existence of a strong frozen component. As can be found in the collective diffusion theory, $g^{(1)}_{\mathrm{F}}(q,\tau)$ is given by

$$g^{(1)}(q,\tau) = f_{\mathrm{HT}}(q,\tau) = \frac{\langle E_{\mathrm{F}}(q,0)E_{\mathrm{F}}{}^*(q,\tau)\rangle_{\mathrm{E}}}{\langle I_{\mathrm{F}}(q,0)\rangle_{\mathrm{E}}} = \frac{\langle E_{\mathrm{F}}(q,0)E_{\mathrm{F}}{}^*(q,\tau)\rangle_{\mathrm{T}}}{\langle I_{\mathrm{F}}(q,0)\rangle_{\mathrm{T}}} = \exp(-D_{\mathrm{HT}}q^2\tau). \quad (33)$$

Note that the ergodic assumption, i.e., $\langle A\rangle_{\mathrm{E}} = \langle A\rangle_{\mathrm{T}}$, is valid here. An apparent diffusion coefficient D_{A} is obtained by taking the slope of the plot of $\ln[g^{(2)}(\tau) - 1]$ vs τ, i.e.,

$$D_{\mathrm{A}} = -\frac{1}{2q^2}\lim_{\tau\to 0}\frac{\mathrm{d}}{\mathrm{d}\tau}\ln\{g^{(2)}(\tau) - 1\}. \quad (34)$$

It is essential to recognize that there is a cutoff at low intensities resulting from the contribution $\langle I_{\mathrm{F}}\rangle_{\mathrm{T}}$. Therefore, $\langle I_{\mathrm{F}}\rangle_{\mathrm{T}}$ is proportional to the thermal energy kT. The population function, $P(\langle I\rangle_{\mathrm{T},p})$, is described as a function of the scattering intensity difference, $\langle I\rangle_{\mathrm{T}} - \langle I_{\mathrm{F}}\rangle_{\mathrm{T}}$,

$$P(\langle I\rangle_{\mathrm{T},p}) \approx H[\langle I\rangle_{\mathrm{T},p} - \langle I_{\mathrm{F}}\rangle_{\mathrm{T}}]\exp\left[-\frac{\langle I\rangle_{\mathrm{T},p} - \langle I_{\mathrm{F}}\rangle_{\mathrm{T}}}{\langle I\rangle_{\mathrm{E}} - \langle I_{\mathrm{F}}\rangle_{\mathrm{T}}}\right], \quad (35)$$

where $H(x)$ is the Heaviside function, i.e., $H(x) = 0$ for $x < 0$ and $H(x) = 1$ for $x \geq 0$. Figure 7c shows $P(\langle I\rangle_{\mathrm{T},p})$ obtained by sorting $\langle I\rangle_{\mathrm{T},p}$ in Fig. 7a. The solid line in the figure is the reconstructed curve with Eq. 35, which fits well with the experimental data. The value of $\langle I\rangle_{\mathrm{T},p}$ at the cutoff is equal to $\langle I_{\mathrm{F}}\rangle_{\mathrm{T}}$. Therefore, the scattering intensity is a sum of $\langle I_{\mathrm{F}}\rangle_{\mathrm{T}}$ (the dashed line), and the uninteresting frozen scattering component, $I_{\mathrm{C}} = \langle I\rangle_{\mathrm{T}} - \langle I_{\mathrm{F}}\rangle_{\mathrm{T}}$. Only the former is relevant, and the latter provides the local oscillator for optical heterodyne detection.[26,44] The diffusion coefficient, D_{HT}, in Eq. 33 is given by

$$D_{\mathrm{HT}} = (2-X)D_{\mathrm{A}} = \frac{\sigma^2_{\mathrm{I}}}{X}D_{\mathrm{A}} \quad (\text{for } 0 < X \leq 1). \quad (36)$$

If $X = 1$, D_{HT} becomes equal to D_{A} and a pure homodyne mode is attained. On the other hand, for $0 < X \ll 1$, D_{HT} approaches $2D_{\mathrm{A}}$, which is the case of a pure heterodyne mode. The relationship between D_{NE} and D_{HT} is given by

$$D_{\mathrm{HT}} = \frac{Y}{X}D_{\mathrm{NE}} = (2-X)D_{\mathrm{A}}. \quad (37)$$

We proposed the following linearized equation by rearranging Eq. 36,[7,45–47]

$$\frac{\langle I\rangle_{\mathrm{T},p}}{D_{\mathrm{A},p}} = \frac{2}{D_{\mathrm{HT}}}\langle I\rangle_{\mathrm{T},p} - \frac{\langle I_{\mathrm{F}}\rangle_{\mathrm{T},p}}{D_{\mathrm{HT}}}. \quad (38)$$

This equation is very useful to extract D ($=D_{\mathrm{HT}}$) and $\langle I_{\mathrm{F}}\rangle_{\mathrm{T}}$. Figure 7d shows the linearized plot of the apparent diffusion coefficient as a function of $\langle I\rangle_{\mathrm{T}}$. Both D and $\langle I_{\mathrm{F}}\rangle_{\mathrm{T}}$ can be precisely evaluated from the slope and the intercept of this plot.

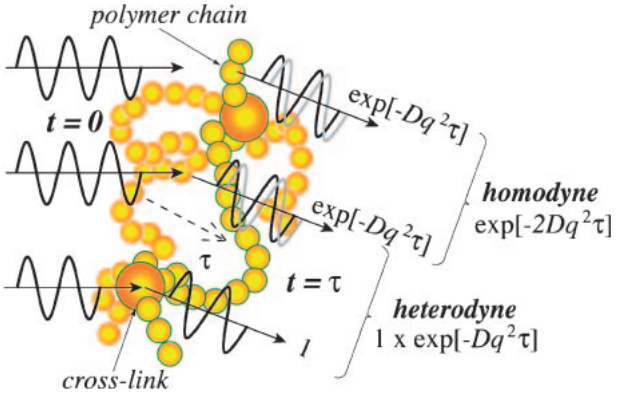

Fig. 8. Schematic illustration of homodyne and heterodyne modes of DLS. Polymer chains move, while cross-links do not. $g^{(1)}(q,\tau)$ is obtained as a product of scattering fields, which becomes either $\exp[-2Dq^2\tau]$ (homodyne) or $\exp[-Dq^2\tau]$ (heterodyne).

Figure 8 schematically illustrates the homodyne and heterodyne modes of DLS. The sample is a gel consisting of polymer chains, cross-links, and solvent. The polymer chains undergo Brownian motion, while the cross-links remain at the same position. A polymer chain at time $t = 0$ moves from the left to the right during τ. The scattering field at a segment of the polymer chain has a decay of $\exp[-Dq^2\tau]$ due to Brownian motion. On the other hand, a cross-link does not produce any decay, i.e., 1, and play as a local oscillator. Since $g^{(1)}(q,\tau)$ is obtained by taking an average of the product of two scattering fields, it becomes either $\exp[-2Dq^2\tau]$ or $\exp[-Dq^2\tau]$, depending on the combination. The former is called homodyne, and the latter is heterodyne. Since a gel has a huge number of local oscillators, i.e., cross-links, or highly cross-linked parts, heterodyne components are not negligible.

This treatment is sometimes too rough, and further refinement of the theories has been carried out by Furukawa and co-worker[48] and by Norisuye et al.[49] Furukawa and Hirotsu discussed the case when dynamic concentration fluctuations also depend on the sample position.[48] Norisuye et al. studied this problem further and concluded that dynamic inhomogeneities are observed for gels with rather high cross-link densities as a result of the difference in the molecular environment, i.e., the difference in the local gel concentrations and/or cross-link density.[49] However, since further discussions on this direction are beyond the scope of this review, we treat the dynamic fluctuations as being position-independent.

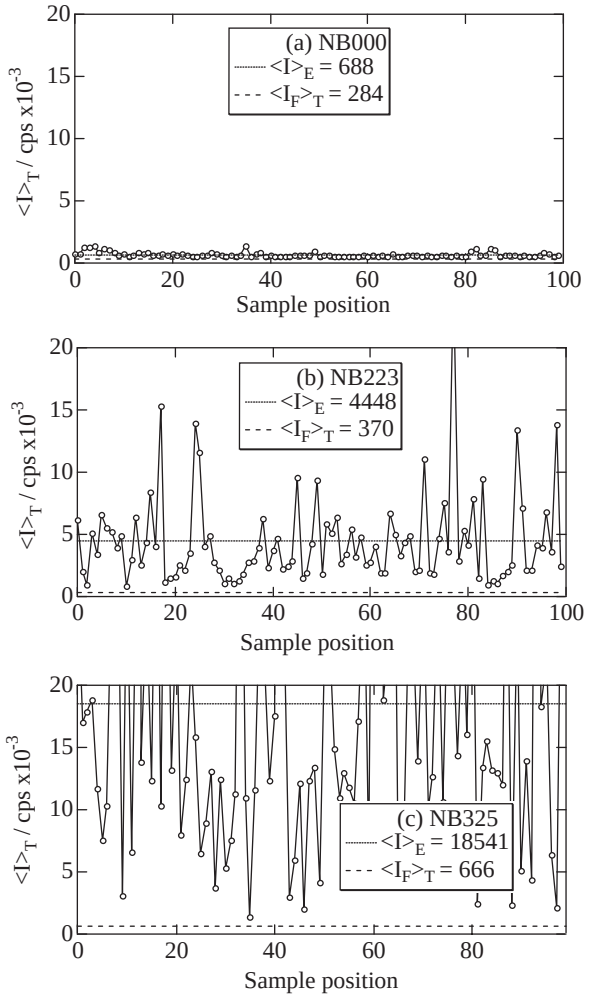

Fig. 9. Cross-linker concentration, C_x, dependence of speckle patterns for PNIPA gels [Reproduced with permission from *Macromolecules* **1996**, *29*, 8746, Copyright permission: American Chemical Society] (Fig. 1).

4. Decomposition of Dynamic Fluctuations and Static Inhomogeneities

It is naively expected that inhomogeneties increase with increasing the cross-kink concentration in a gel. As a matter of fact, Mallam et al. observed that SAXS intensity increases with an increase in concentration of the cross-linker in PAAm hydrogel cross-linked with *N*,*N*′-methylenebisacrylamide (BIS).[28] The SAXS intensity profiles correlate to the scattering intensity functions obtained by light scattering. This example suggests that inhomogeneities increase with increasing cross-links. How about the effects of polymer concentration, temperature, and the degree of dissociation? What happens if the environment of a gel changes after gel preparation? In this section, these questions are discussed based on several examples. According to de Gennes,[42] the structure of gels is determined with two ensembles: "preparative ensemble" (state at preparation) and "final ensemble" (state at observation). As a matter of fact, the structure of gels must be characterized not only with environmental parameters at observation but also with those at preparation.

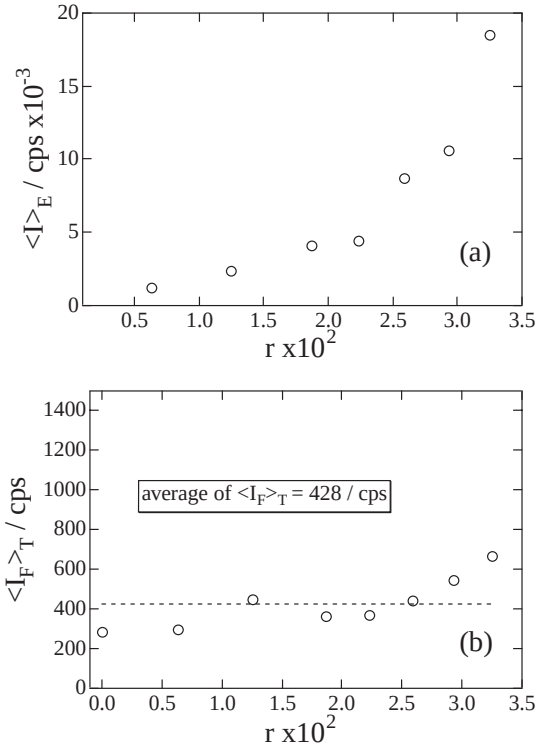

Fig. 10. Cross-linker concentration ratio, $r = C_x/C_{NIPA}$, dependence of $\langle I\rangle_E$ for PNIPA gels [Reproduced with permission from *Macromolecules* **1996**, *29*, 8746, Copyright permission: American Chemical Society] (Fig. 5).

PNIPA hydrogels and their copolymer gels with ionizable comonomer, such as acrylic acid (AAc), are extensively investigated because PNIPA hydrogels are very sensitive to their environment, such as temperature, pH, pressure, etc.[6] It should be also noted that PNIPA hydrogels are more chemically stable against hydrolysis than PAAm hydrogels because the isopropyl group stabilizes the amide carbon against the attack of OH^-.[50] PAAm hydrogels are easily hydrolyzed, and the amide groups are substituted by hydroxy groups, which results in a significant change in the inhomogeneities as well as swelling behavior.[51]

4.1 Gel Composition and Environmental Parameter Dependence. Figure 9 shows speckle patterns obtained from PNIPA hydrogels.[45] The cross-linker (BIS) concentration, C_{BIS}, was varied from 0 to 325 mM, while the NIPA monomer concentration, C_{NIPA}, was fixed to 690 mM. As shown in the figure, the speckle patterns become stronger with C_{BIS}. The ensemble-average scattering intensity, $\langle I\rangle_E$, and $\langle I_F\rangle_T$ were obtained with the method described in Section **3**. The variations of $\langle I\rangle_E$ and $\langle I_F\rangle_T$ with C_{BIS} are shown in Fig. 10, where the ratio of the cross-linker to the monomer, $r \equiv C_{BIS}/C_{NIPA}$, was chosen as a measure of cross-linker concentration. As expected, $\langle I\rangle_E$ increases with r, while $\langle I_F\rangle_T$ was rather independent of r as shown with the dashed line.

Effects of charged comonomer on inhomogeneities are also interesting. Figure 11 shows variations of speckle patterns with (a) temperature, and (b) the comonomer concentration, C_{AAc}, in PNIPA/AAc copolymer gels.[46] Since PNIPA in water has a lower-critical solution temperature (LCST) around

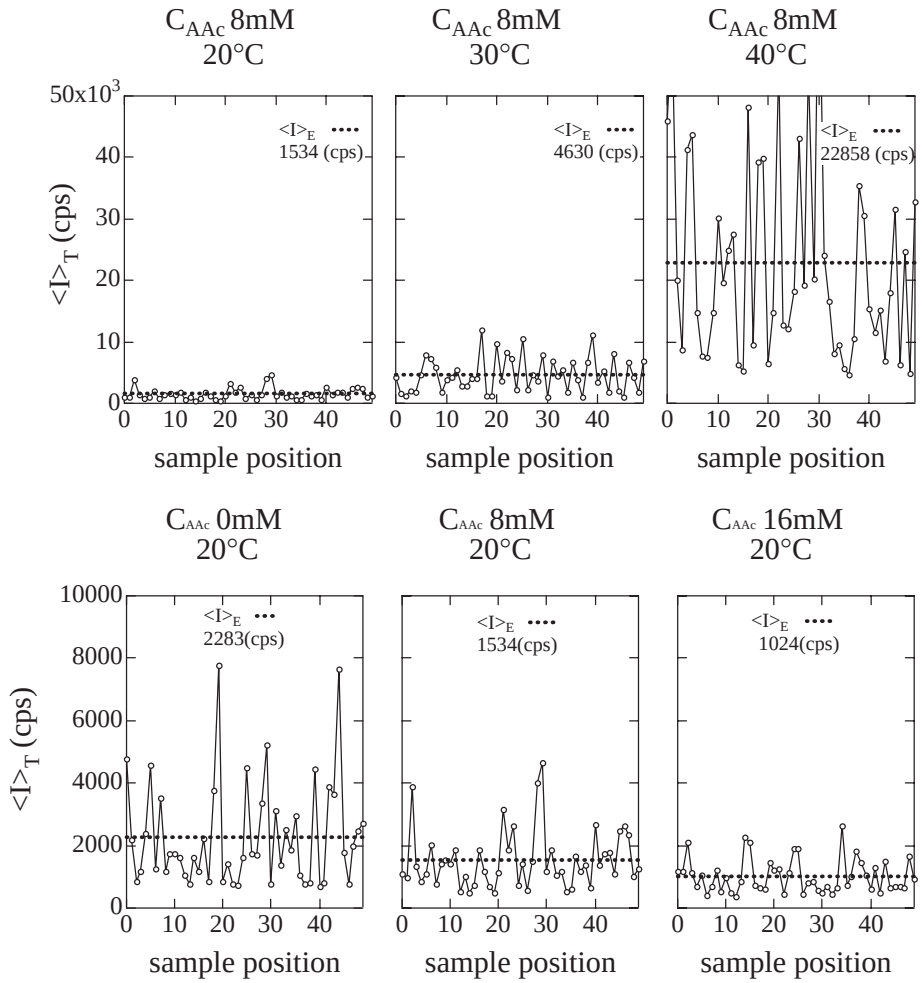

Fig. 11. Temperature and comonomer concentration, C_{AAc} (AAc; acrylic acid), dependence of the speckles and $\langle I \rangle_E$ for PNIPA/AAc copolymer gels [Reproduced with permission from *Macromolecules* **1996**, *29*, 6535, Copyright permission: American Chemical Society] (Figs. 2 and 3).

32 °C,[5,6] the increase in inhomogeneities, $\langle I \rangle_E$ (the dashed line), with T observed in the PNIPA/AAc gels is easily understood. On the other hand, the decrease in $\langle I \rangle_E$ with C_{AAc} is ascribed to an increase in osmotic pressure by ionization. However, effects of charges on gel inhomogeneities are complicated issues as extensively investigated by Ikkai et al.[23,30,52,53]

Inhomogeneities also vary by changing monomer concentration, C_{NIPA}. Figure 12 shows C_{NIPA} dependence of $\langle I \rangle_E$.[54] Interestingly, $\langle I \rangle_E$ of as-prepared gels (i.e., reactor-batch gels) decreases with increasing C_{NIPA}. Furukawa et al. observed a similar result.[55] This is due to the fact that concentration fluctuations are suppressed by increasing the solute concentration. However, more surprisingly, Figure 12 also shows that $\langle I \rangle_E$ increases with swelling (from closed to open circles). Since swelling means a lowering of concentration and a lowering of scattering elements in a system, a decrease in scattering is expected. However, the experimental result suggests that such speculation is incorrect. The reason of the increase in $\langle I \rangle_E$ by swelling is ascribed to the nature of inhomogeneities.

Bastide and Leibler schematically depicted this phenomenon (Fig. 13).[56] Dots represent interchain cross-links and thick lines indicate clusters of first chemical neighbor junctions (frozen blobs) which do not swell. According to this model, cross-

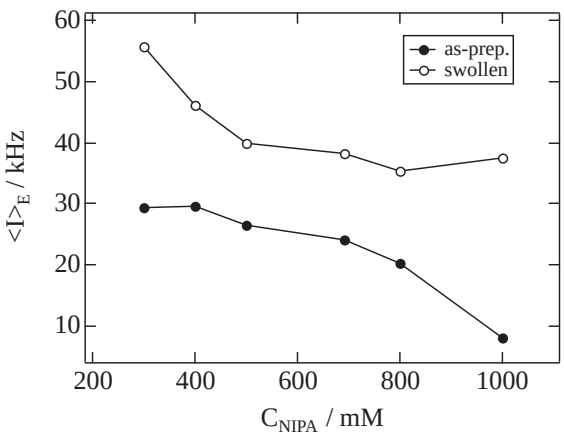

Fig. 12. Polymer concentration, C_{NIPA}, dependence of $\langle I \rangle_E$ for PNIPA gels in the as-prepared state (reactor-batch; filled circles) and in the equilibrium swollen state (open circles) [Reproduced with permission from *J. Chem. Phys.* **2000**, *112*, 442, Copyright permission: American Institute of Physics] (Fig. 3).

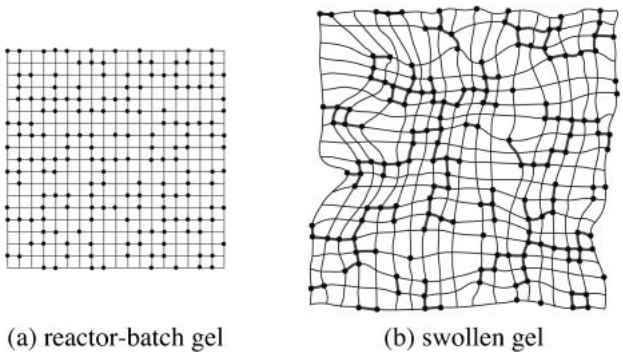

Fig. 13. Model of gel networks for (a) a reactor-batch gel and (b) a swollen gel. Dots represent interchain cross-links and thick lines indicate clusters of first chemical neighbor junctions (frozen blobs) which do not swell [Reproduced with permission from *Macromolecules* **1988**, *21*, 2647, Copyright permission: American Chemical Society] (Fig. 1).

linking inhomogeneities are hidden by the neighboring network chains with the same monomer concentrations. However, swelling leads to a dilution of the network preferentially in a low-cross-linked part of the network, resulting in an increase in inhomogeneities.

$\langle I_F \rangle_T$ and D were found to decrease and increase, respectively, with increasing the polymer volume fraction, ϕ, as shown in Fig. 14, where ϕ varied rather linearly with C_{NIPA}.[54] D increases with ϕ for both types of gels. Joosten et al.[44] reported an increase of D with increasing polymer concentration for reactor-batch acrylamide gels. The reported values of D's are in good agreement with our results. Note that D's for the swollen gels are larger than for the reactor-batch gels for a given value of ϕ. The ϕ dependence of D can be analyzed with a power law behavior, i.e., $D \approx \phi^s$. However, the exponent $s = 3/4$, predicted for a semidilute solution in the scaling regime,[42] was not obtained in this system. The estimated exponents were 0.53 and 0.63 for the reactor-batch and swollen gels, respectively, as shown in the insets. This is due to the fact that the concentration regime studied here is in the crossover regime.

Pressure dependence of gel structure and dynamics is also an interesting subject. Nakamoto et al.[57] studied preparation pressure, P_{prep}, dependence of PNIPA gel inhomogeneities and found that $\langle I \rangle_E$ diverged by approaching the spinodal pressure, P_{sp} ($\approx$168 MPa), which is similar to temperature-driven critical phenomena. Shibayama et al. investigated pressure dependence of PNIPA gels by SANS as a function of observation pressure, P_{obs}.[58] It was found that the inhomogeneities

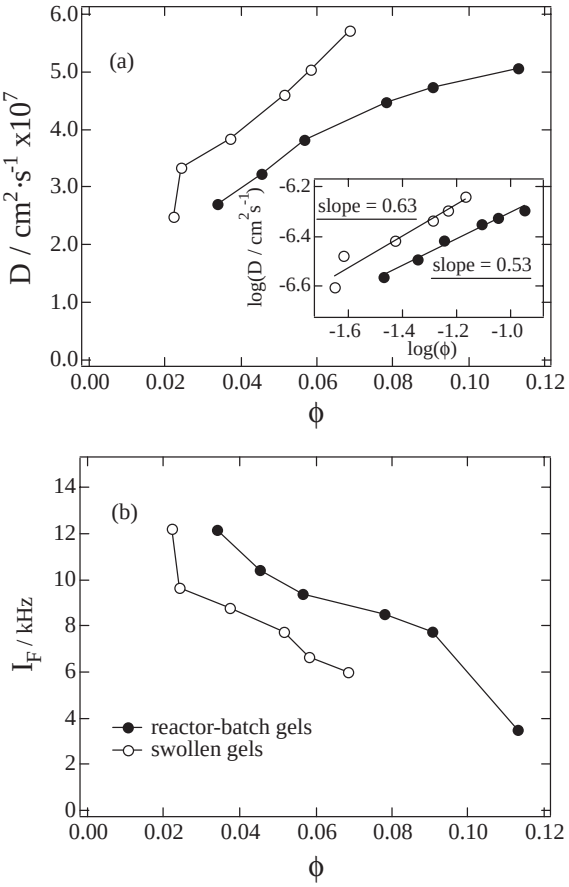

Fig. 14. Polymer fraction, ϕ, dependence of D and $I_F = \langle I_F \rangle_T$ for PNIPA gels in the as-prepared state (reactor-batch; filled circles) and in the equilibrium swollen state (open circles) [Reproduced with permission from *J. Chem. Phys.* **2000**, *112*, 442, Copyright permission: American Institute of Physics] (Fig. 8).

increased with increasing P_{obs} at lower temperatures than LCST of PNIPA-water. However, a parabolic phase diagram was obtained having a maximum around 50 MPa for PNIPA solutions and 100 MPa for PNIPA gels.

Table 1 summarizes the parameter dependence of D, $\langle I_F \rangle_T$, and $\langle I \rangle_E$. It is clear from this table that (1) the dynamic fluctuations originate from the concentration fluctuations independent of cross-link concentration, C_X, (2) the static inhomogeneities depend both on the state of sample preparation and on the state of observation, and (3) the dynamic properties do not depend on the state of observation. An increase in the degree

Table 1. Parameter Dependence of Dynamic Fluctuations and Static Inhomogeneities

	Dynamic fluct.		Static inhomo.	References
	D	$\langle I_F \rangle_T$	$\langle I_C \rangle_E$	
Cross-linker conc. C_x	↑	—	↑	*Macromolecules* **1996**, *29*, 8746
Polymer conc. C	↑	↓	↓	*J. Chem. Phys.* **2000**, *12*, 442
Deg. of Ionztn. f	↑	↓	↓	*Macromolecules* **1996**, *29*, 6535
Prep. temp. T_{prep}	—	—	↑	*Physica A* **1998**, *249*, 245
Obs. temp. T_{obs}	↓	↑	↑	*Physica A* **1998**, *249*, 245
Prep. pressure P_{prep}	—	—	↑	*Macromolecules* **2001**, *34*, 911
Obs. pressure P_{obs}	↑↓	—	↑↓	*Macromolecules* **2004**, *37*, 2909

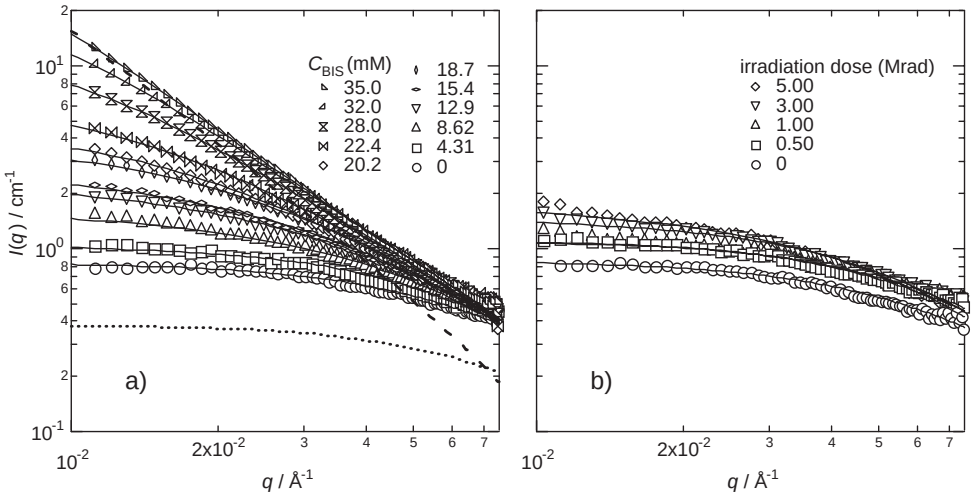

Fig. 15. SANS intensity functions for (a) BIS gels and (b) γ-ray cross-linked gels with various BIS concentrations, C_{BIS}, and γ-ray doses, respectively. The dotted and dashed lines are the fits with Panyukov–Rabin theory [Reproduced with permission from *Polymer* **2002**, *43*, 5289, Copyright permission: Elsevier] (Fig. 3).

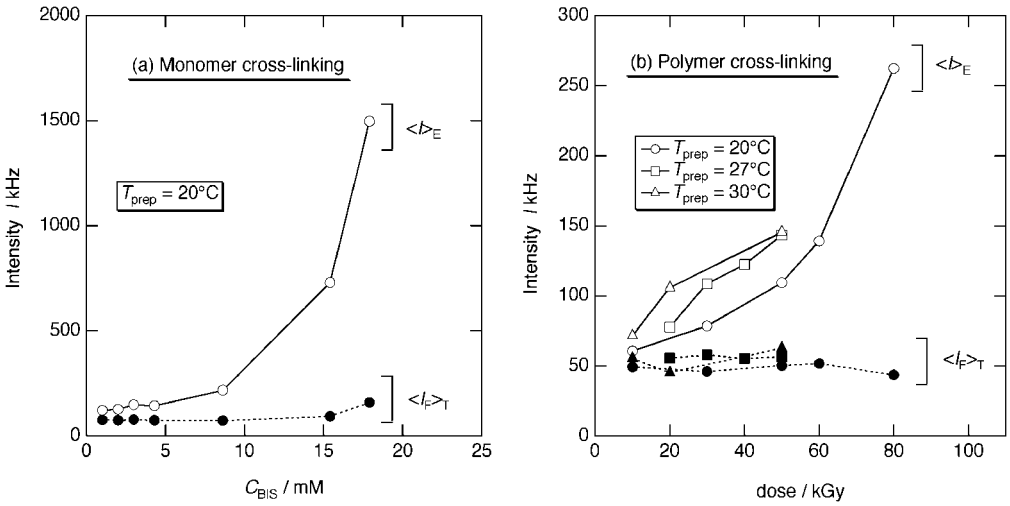

Fig. 16. C_{BIS}, and γ-ray doses dependence of $\langle I\rangle_E$ and $\langle I_F\rangle_T$ for (a) monomer cross-linked and (b) polymer cross-linked gels [Reproduced with permission from *Macromolecules* **2003**, *36*, 6202, Copyright permission: American Chemical Society] (Fig. 8).

of ionization, f, increases the osmotic pressure, resulting in an increase in D and suppression of both of dynamic and static concentration fluctuations. An extensive review of charge effects is given by Ikkai and Shibayama.[23]

4.2 Radiation Cross-Linked Gels. Chemical gels are usually obtained by polymerizing a monomer in the presence of a cross-linker. Hereafter, we call them monomer cross-linked gels. In this case, the reaction chemistry determines the microscopic structure of the gel. Polymer gels obtained by radiation cross-links (polymer cross-linked gels), on the other hand, are expected to be more homogeneous than monomer cross-linked gels because cross-linking reaction can be done without perturbing the concentration fluctuations of the pregel solution. Figure 15 shows SANS intensity curves obtained for (a) monomer cross-linked (BIS) gels and (b) polymer cross-linked (γ-ray irradiated) gels.[34] It is clear from the figure that the monomer cross-linked gels are much more inhomogeneous than the polymer cross-linked gels. The solid, dashed, and dotted lines denote the calculated curves for $S(q)$ (the total structure factor), $C(q)$ (the frozen inhomogeneities), and $G(q)$ (the dynamic inhomogeneities), respectively, based on the Panyukov–Rabin theory (see Eqs. 4–6).[20]

Figure 16 shows a comparison of $\langle I\rangle_E$ and $\langle I_F\rangle_T$ of (a) monomer cross-lined gels and (b) polymer cross-linked gels as a function of cross-linker concentration.[59] Note that the scale of the ordinate is about ten times different. This figure also clearly indicates that the monomer cross-linked gels are more inhomogeneous. Another interesting feature is that $\langle I\rangle_E$ of polymer cross-linking also depends on T_{prep}, similar to the case of monomer cross-linking. Figure 17 schematically illustrates the difference of the network structure.[59] For the polymer cross-liking system, chains are loosely connected together but remain in sol state at low cross-linking degree (Fig. 17a). With increasing irradiation dose, a γ-ray gel having random distribution of cross-links are formed as shown in Fig. 17b. On the other hand, a larger amount of cross-links are required to form a gel for the monomer cross-linking system because of cross-liking formation by intra-cross-linking and/or difference

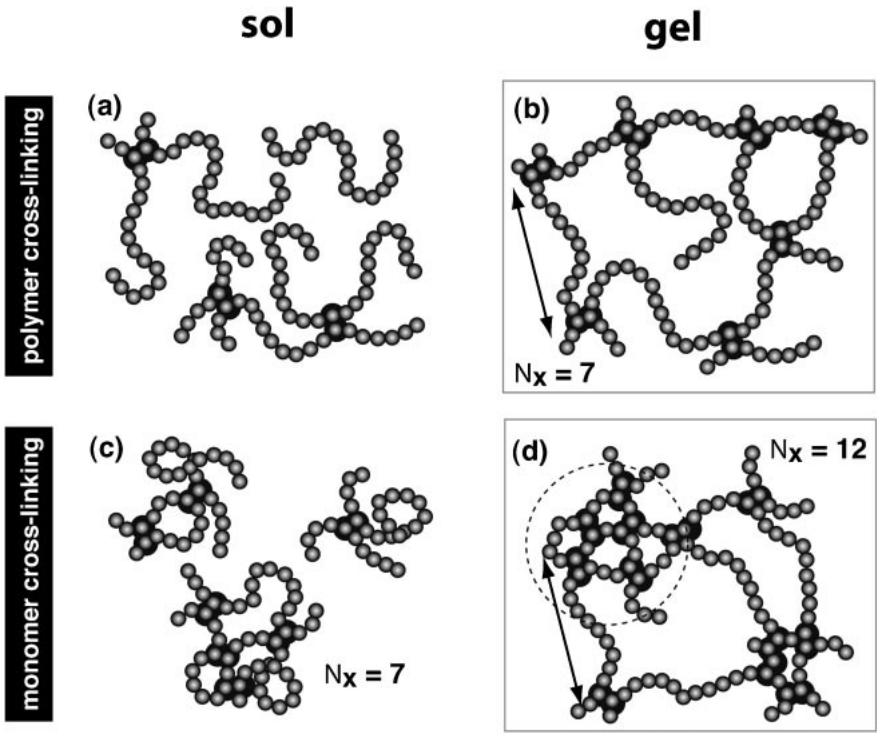

Fig. 17. Schematic representation of the network structure of PNIPA gel cross-linked with (a) BIS and (b) γ-ray irradiation [Reproduced with permission from *Macromolecules* **2003**, *36*, 6202, Copyright permission: American Chemical Society] (Fig. 4).

of monomer reactivity ratio between monomer and cross-linker. Thus, as shown in Fig. 17c, a gel cannot be formed with the same number of cross-links, say $N_X = 7$, with (b) as indicated by N_X. When further cross-links ($N_X = 12$) are introduced (d), the clusters are interconnected together, resulting in infinite network formation. The monomer cross-linking gels have almost the same distance between cross-links as indicated by arrows, but the cross-linker rich domains are incorporated in the structure, resulting in higher average cross-linking density.

4.3 Inhomogeneities and Gel Shrinking. Striking is a feature of inhomogeneites and affects the physical properties of gels. Figure 18 shows the time course of swelling ratio, d/d_0, for (a) the PNIPA monomer cross-linked gels and (b) the γ-ray cross-linked gels with different cross-linking concentrations, after a T-jump from 20 to 45 °C, where d is the diameter of the gel at observation and d_0 is the capillary diameter at which the gel was formed.[59] As can be seen from the figure, rapid shrinking was attained by simply lowering the cross-linker concentration or the irradiation dose for both types of gels indicated by filled symbols. A similar result has been reported for monomer cross-linked gels. An abrupt change from rapid to slow shrinking was found around $C_{BIS} = 8.62$ mM for the monomer cross-linked gels and around irradiation dose of 40 kGy for the γ-ray irradiated gels. Two-step shrinking was also observed for both gels at the critical cross-linking density for the rapid shrinking, i.e., 8.62 mM and 40 kGy. Although the unit of cross-linking degree was different in the two types of gels, the following relation was obtained from the critical densities in this study as,

$$[\text{irradiation dose (kGy)}] = 4.64 \times [C_{BIS}\ (\text{mM})], \quad (39)$$

for the PNIPA gels with $T_{prep} = 20$ °C. There are two possible explanations for a two-step reduction in the swelling ratio. One is a formation of the skin layer, and the other is a two-step shrinking via crumpled globule formation proposed by Grosberg and Nechaev[60] and by Dawson et al.,[61,62] i.e., chain shrinking and subsequent intra-cluster association. Let us first discuss the first possibility in more detail.

When a gel is immersed in hot water, the temperature of the gel increases above the transition temperature, resulting in phase separation followed by gel shrinking. However, shrinking can take place only at the surface and the inner part of gels is not allowed shrinking because out-going water is blocked by surface shrinking, i.e., skin formation. Therefore, skin formation plays a major role in slow shrinking as discussed in the literature.[63] The thickness of the skin, r_{skin}, is obtained by,[59]

$$r_{skin} = \frac{d_0}{2}\left(d_2 - \sqrt{\frac{d_3^3 d_1^2 - d_1^3 d_2^2}{d_3^3 - d_1^3}}\right). \quad (40)$$

Here, ϕ_i and d_i are the polymer volume fraction and the diameters, respectively, as defined in Fig. 18. In this case, r_{skin}s for the monomer cross-linking and polymer cross-linking systems were evaluated as 2.50 and 3.44 μm, respectively. The second possibility is that the initial chain shrinking and subsequent intra-cluster association. However, the second possibility, i.e., the two-step shrinking via crumpled globule formation, does not seem to be adequate for the rapid shrinking because it requires macroscopically homogeneous shrinking as is the case of dilute polymer solutions. Therefore, we expect that skin-layer formation is the reason of two-step shrinking, and skin layer formation is one of major criteria for slow shrinking kinetics. Despite the different cross-linking methods, both gels exhibit a similar shrinking kinetics.

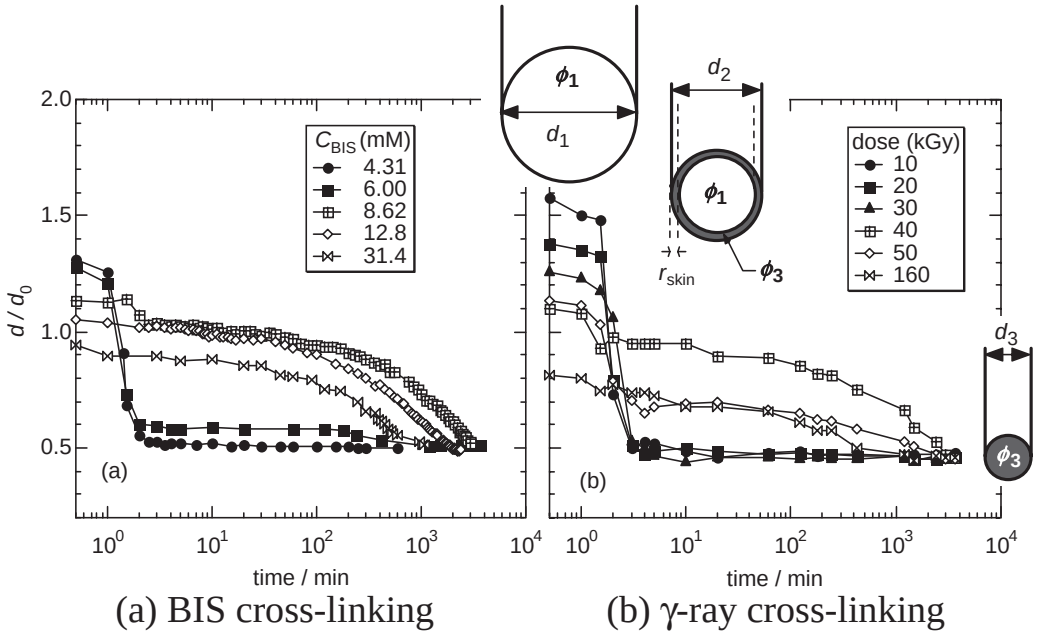

Fig. 18. Comparison of shrinking kinetics between (a) chemically cross-linked (BIS cross-linked gel) and (b) γ-ray cross-linked gel [Reproduced with permission from *Macromolecules* **2003**, *36*, 6202, Copyright permission: American Chemical Society] (Fig. 1).

Gel preparation temperature, T_{prep}, also affects the shrinking kinetics. Figure 19a shows optical photographs for PNIPA gels in regime I to IV undergoing shrinking transition after a T-jump from 20 to 45 °C.[64] The shapes of gels during shrinking process greatly depend on T_{prep}. The gel prepared at 20 °C (regime I) was transparent after 2 min of T-jump, and the size did not change much in 2 min. Characteristic bubble formation took place for the gel at $T_{prep} = 26.0$ °C (regime II), which also occurs in PNIPA gels with lower C_{BIS} ($\leq$4 mM) or C_{NIPA} ($\leq$400 mM), or in the case of a higher destination temperature for the T-jump.[65] By further increasing T_{prep} (regime III), quick shrinking leads to a collapse of gel with an irregular shape. The gel with $T_{prep} = 31.5$ °C underwent a clear-to-opaque transition accompanied by transformation to an irregular shape. Regime IV is characterized by isotropic shrinking by keeping the original shape. In regime IV, the gel was inherently opaque, indicating phase separation. This phase separation leads to a rapid shrinking.

Figure 19b schematically illustrates T_{prep} dependence of the network structures before and after swelling. When a PNIPA gel is formed at a low temperature ($T \leq 20$ °C), the network structure is rather homogeneous. The gel can swell uniformly by immersing in deionized water at the observation temperature $T_{obs} = 20$ °C. However, gels prepared at higher temperatures, the network structure becomes inhomogeneous due to the LCST nature of PNIPA aqueous systems, resulting in a formation of polymer-rich domains or aggregates in the matrix of loosely tied network. The domains are connected with "tie-chains" as shown in the figure (regime II and III) and form a loose network. It is expected that these domains are hard to swell because of high polymer density and cross-linking, whereas the matrix part is capable of swelling as discussed by Bastide and Leibler.[56] This is why a larger swelling ratio is observed for the gel prepared at higher T_{prep}. By further increasing T_{prep} (regime IV), however, gels lose tie-chains, and a large portion of condensed domains loses inter-domain connection. These gels look opaque due to phase separation. Therefore, these types of gels lose their swelling capability.

4.4 The Spatial Extent of Inhomogeneities. Are inhomogeneities in a gel inherent of the length of observation? The answer is no. The characteristic size of inhomogeneities in gels is usually much smaller than the wavelength of visible light. This is why there exist many clear gels containing a high degree of inhomogeneities. To demonstrate this fact, it is interesting to display the degree of inhomogeneities as a function of q. Figure 20a shows the inverse of inhomogeneities, $\langle I_F \rangle_T / \langle I \rangle_E$ (evaluated by light scattering, LS) and $G(q)/S(q)$ (evaluated by SANS), plotted as a function of q.[33] The variable $G(q)/S(q)$ is the ratio of the structure factor corresponding to the dynamic fluctuations and the total structure factor, respectively. On the other hand, the ratio $\langle I_F \rangle_T / \langle I \rangle_E$ was obtained by LS at a fixed angle of 90°. As shown in the figure, the inverse of the degree of inhomogeneities vary with q. In addition, the inhomogeneities become insignificant as q increases. The physical meaning of this fact can be explained with Fig. 20b. With the scale length lower than the mesh size, i.e., the inter-cross-link distance, there are no inhomogeneities introduced by cross-links. Therefore, the effect of C_X is more significant in the LS region than in the SANS region. This indicates that gel inhomogeneities are strongly affected by C_X. Hence, it can be concluded that the control of inhomogeneity is very important if gels are to be used in optical devices, such as contact lens.

5. Inhomogeneities in Thermoreversible Physical Gels

In the previous sections, we discussed that nonergodic media, such as glasses and gels, have frozen spatial inhomogeneities due to a frozen structure (in glasses) or topological constraints, i.e., cross-linking (in gels). One clear manifestation of nonergodicity is the appearance of speckles. It has generally been believed that spatial inhomogeneities are characteristic

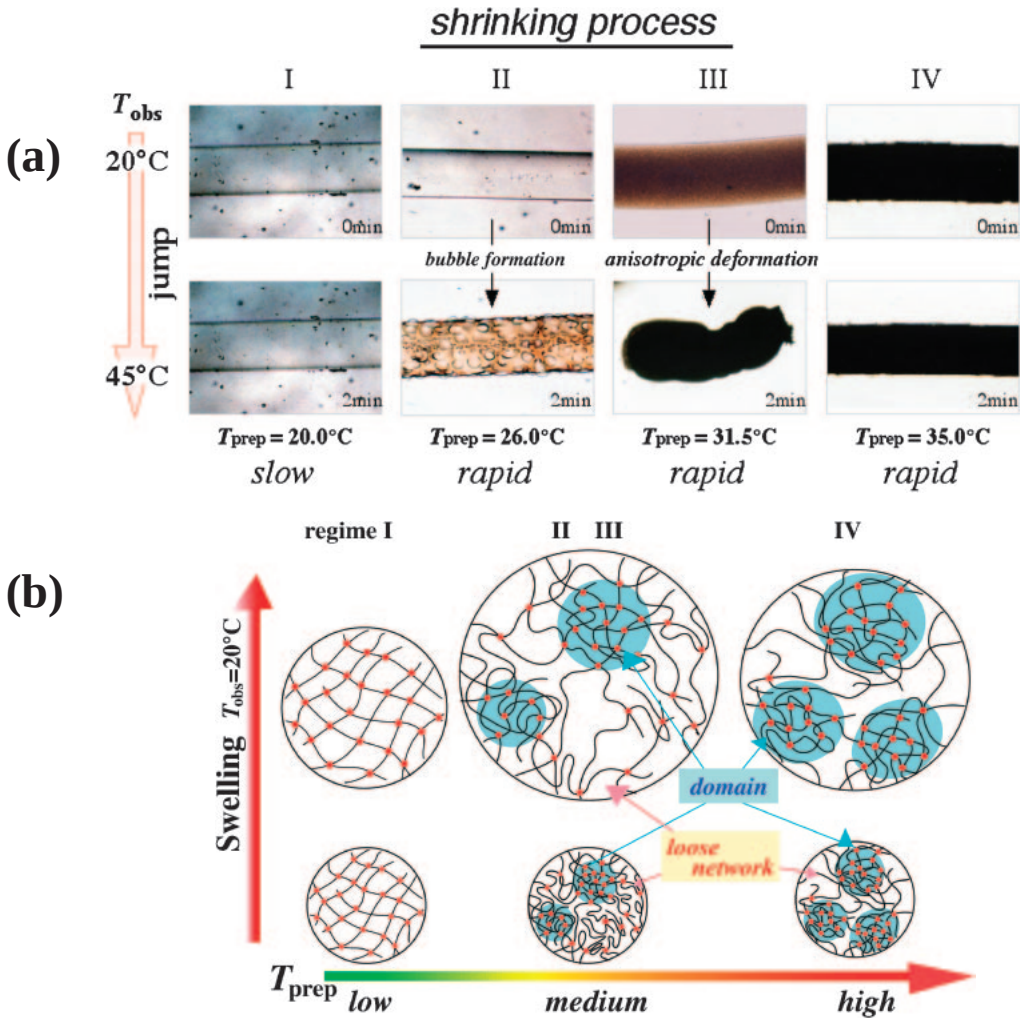

Fig. 19. (a) Photographs showing cylindrical gels before and 2 min after T-jump from 20 to 45 °C. Characteristic bubbles were formed exclusively in the gel in regime II. T_{prep} was varied from I to IV. (b) Schematic illustration of PNIPA gel networks prepared at different T_{prep}'s [Reproduced with permission from *Polymer* **2002**, *43*, 3101, Copyright permission: Elsevier] (Figs. 5 and 8).

features of chemical gels and that the speckles are not observed in physical gels. The following two examples clearly demonstrate that the above hypothesis is incorrect.

5.1 PVA/CR Gels. The first observation of speckle appearance/disappearance in thermoreversible physical gels was made in poly(vinyl alcohol)/Congo Red (PVA/CR; $C_{32}H_{22}N_6Na_2O_6S_2$) aqueous solutions.[66] PVA/CR hydrogels were chosen because of the following reasons: (1) gelation is governed by chemical equilibrium and hence the rate is quick enough (a few minutes) without hysteresis; (2) the sol–gel transition temperature, T_{gel}, is located at a temperature for easy handling, i.e., ≈43 °C; and (3) the sol–gel phase diagram,[67] the microscopic structure,[68] and its enthalpy of gel melting are well characterized. PVA/CR is a kind of "slime" with which children play.[69] Although "slime" is usually made of laundry starch (PVA) and borax, i.e., hydrated sodium borate, PVA/borax aqueous solutions are thermoreversible gels and their sol–gel transition has been extensively invesitigated.[70–73]

PVA (the degree of polymerization and the degree of saponification being 1800 and 99.96 mol %, respectively) was dissolved in boiling distilled water and filtered with a 0.2 μm filter. Aqueous solution of reagent grade CR, a synthetic dye, was added to the PVA solution. CR acts as a cross-linker of PVA via hydrogen bonding between $-NH_2$ group of CR and –OH group of PVA. The sol–gel transition temperature was determined to be $T_{gel} \approx 43$ °C by flow measurement. The sol–gel phase diagram is shown in Fig. 21a.[67] As shown here, the sol–gel transition has a re-entrant feature with respect to C_{CR} in the concentration regime of $0.45 \leq C_{PVA} \leq 0.75$ M.[67] This is due to ionization of PVA chains to form a diol structure, followed by formation of di-diol structure as discussed elsewhere.[74] As a mater of fact, Figure 21b shows a series of photographs of PVA/CR showing a sol–gel–sol transition. The meniscus is horizontal for the sols. Apart from the details, the most important feature is that the sol–gel transition behavior is directly correlated to the appearance/disappearance of speckle patterns (Fig. 21c). This clearly indicates that speckles can be used as a signal for gelation not only for chemical gels but also for physical gels. Decomposition of the scattering intensity to those from $\langle I_F \rangle_T$ and static inhomogeneities was successfully carried out in the same manner employed for chemical gels. It was found that $\langle I_F \rangle_T$ is rather temperature independent, and the speckle is solely due to the static inhomogeneities. We believe physical gels have many common features with glasses, and

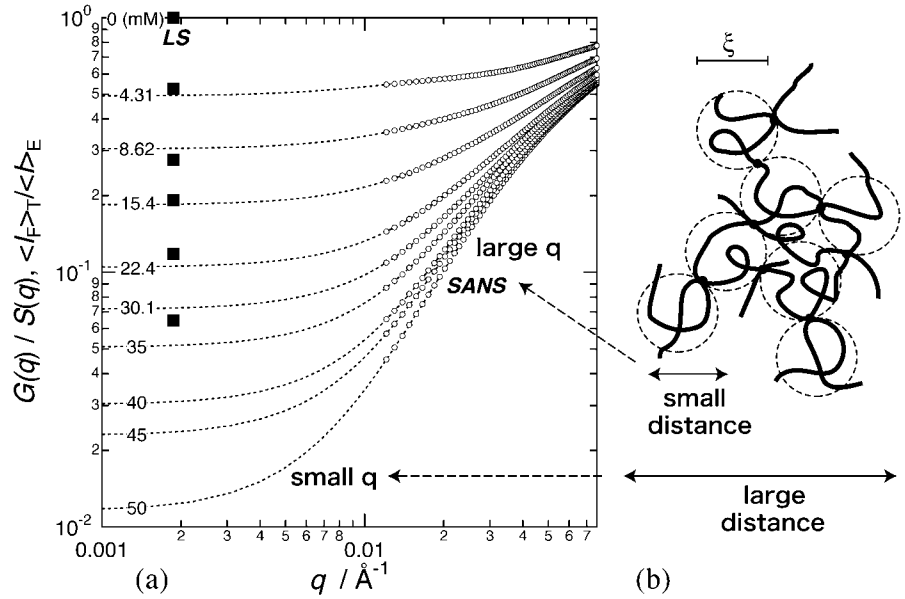

Fig. 20. Ratio of the dynamic fluctuations to the total concentration fluctuations, $G(q)/S(q)$ (for SANS) and $\langle I_F\rangle_T/\langle I\rangle_E$ (for DLS) evaluated for PNIPA gels. The solid squares and open circles are the data obtained by LS and SANS, respectively. The dotted lines are the calculated curves by Panyukov–Rabin theory [Reproduced with permission from *Macromolecules* **2002**, *35*, 4779, Copyright permission: American Chemical Society] (Fig. 7).

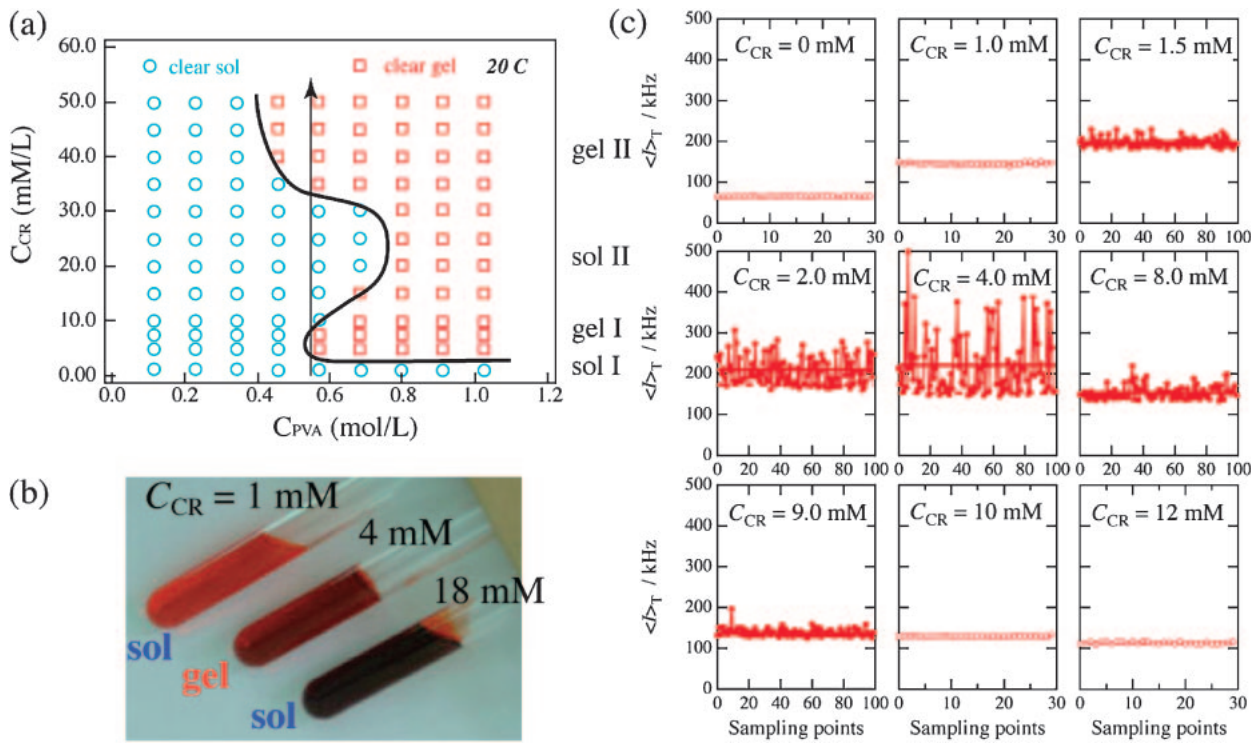

Fig. 21. (a) Phase diagram, (b) photographs, and (c) speckle patterns, showing sol–gel–sol transition with increasing C_{CR}. Speckle patterns (marked in filled circles) appear exclusively in a gel state [Reproduced with permission from *Macromolecules* **2002**, *35*, 1342, Copyright permission: American Chemical Society] (Figs. 2, 3, and 7).

the glassy inhomogeneities in gels will give rise to such universality as has been found in glass-forming systems.

5.2 Gelatin Gels. Another example of a thermoreversible gel is gelatin gel. Gelatin aqueous solutions have long attracted the interest of chemists, physicists, and food scientists because of not only its wide range of applications, such as food, cosmetics, photography, pharmacology, and glues, but also its familiarity as a model system of sol–gel transition.[75] Pioneering works on the structure analysis of gelatin aqueous systems by dynamic light scattering (DLS) were carried out in 1980s in gel state by Hwang and Cummins[76] and in sol state by Amis and co-workers.[77] The presence of collective diffusion mode

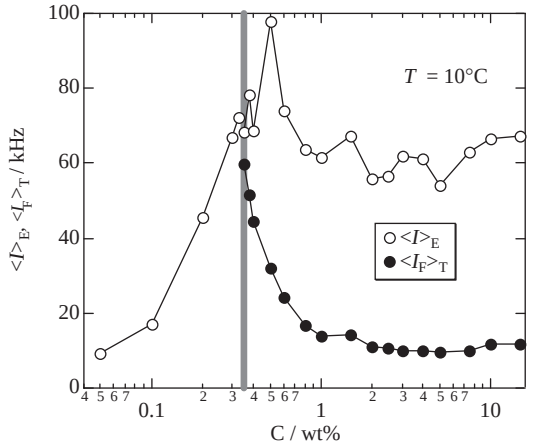

Fig. 22. Results of decomposition for thermoreversible gelatin gel as a function of concentration [Reproduced with permission from *J. Chem. Phys.* **2001**, *115*, 4285, Copyright permission: American Institute of Physics] (Fig. 7).

was reported, and the presence of strong influence of the static component in the scattered intensity was discussed.[76] Amis et al. determined scaling laws for the collective and the slow modes mainly in the sol state of gelatin. A similar conclusion was also drawn by Herning et al.[78] Structural investigations with static light scattering and SANS were carried out by Pezron et al.,[79] and parameters, such as the molecular weight, the radius of gyration, and the second virial coefficient, were evaluated.

Figure 22 shows the results of decomposition with the method proposed in Section **3** for gelatin gels with various concentrations studied at 10 °C. The vertical shaded region denotes the gelation threshold (C_{gel}). Interestingly, $\langle I\rangle_E$ increases with C, up to C_{gel}, and then gradually decreases with C. Note that $\langle I_F\rangle_T$ is equal to $\langle I\rangle_E$ for $C \leq C_{gel}$ because of the system being ergodic in sol state. On the other hand, $\langle I_F\rangle_T$ has a peak at $C = C_{gel}$ and then decreases steeply with a further increase in C, which is related to the space filling of the gelatin clusters and is analogous to the vapor–liquid transition at which critical opalescence appears.[80] The appearance of the plateau region in $\langle I\rangle_E$ is accounted for by suppression of the concentration fluctuations with C. Note that $\langle I\rangle_E$ usually increases with increasing cross-link density.[45] However, in the case of physical gels, such as gelatin, the cross-link density is automatically fixed at a given temperature and concentration. When the ratio of cross-link concentration to the polymer concentration is constant, $\langle I\rangle_E$ was confirmed to be a decreasing function of C.[81] In the case of gelatin gel, such a relation may hold for a given temperature, e.g., 10 °C. A temperature dependence has also been observed.[82]

6. Gel Point Determination and Classification of Gelation

6.1 Time-Resolved DLS. The above discussions suggest that a gelation threshold can be determined by light scattering. The characteristic feature of gelation threshold is the appearance of nonergodicity due to non-cancellation of concentration fluctuations above the threshold. This leads to an increase in the scattering intensity. Furthermore, it has known that $g^{(1)}(\tau)$ and $g^{(2)}(\tau)$ have a long tail with a specific exponent at the gelation threshold,

$$g^{(2)}(\tau) - 1 = \sigma_I^2 \left\{ A \exp(-Dq^2\tau) + \frac{(1-A)}{[1+(\tau/\tau^*)]^{(n-1)/2}} \right\}^2, \tag{41}$$

where A ($0 \leq A \leq 1$) is the fraction of collective diffusion, and σ_I^2 is the initial amplitude of the correlation function. τ^* and n are the characteristic decay time and an exponent related to the dynamics of gels, respectively.[83,84] At the gelation threshold, τ^* becomes infinite. Though the physical meaning of n was discussed by Adam and Lairez[84] and by Muthukumar and Winter,[85] it is not clearly understood.

σ_I^2 is unity for ergodic systems but is less than unity for nonergodic systems. Since $g^{(1)}(q,\tau)$ is obtained by Laplace transform of the distribution function for the decay time, $G(\Gamma)$,

$$g^{(1)}(q,\tau) = \int_0^\infty G(\Gamma) e^{-\Gamma\tau} d\Gamma, \tag{42}$$

a power-law behavior of $g^{(1)}(q,\tau)$ or $g^{(2)}(q,\tau)$ means that $G(\Gamma)$ becomes broad at the gelation threshold. Hence, the characteristic features of the gelation threshold can be summarized as (1) the appearance of speckle patterns or a steep increase in $\langle I\rangle_T$, (2) a lowering of the initial amplitude of the time-intensity correlation function, (3) a power-law behavior in $g^{(1)}(q,\tau)$ and $[g^{(2)}(q,\tau) - 1]$, and (4) a broadening of $G(\Gamma)$. Figure 23 is a typical example showing the four characteristic features of gelation threshold.[22] Time-resolved DLS (TRDLS) experiments were carried out on a mixture of NIPA and tetramethoxysilane aqueous solutions during gelation.[86] The gelation threshold was determined to be $t \approx 16.7$ h in this particular case. The details of the analysis of gelation threshold is given elsewhere.[22]

6.2 Gelators. Gelators are low-molecular weight organic materials, which are able to immobilize organic solvents.[87,88] The first criterion for a gelator is that it must be soluble in the target solvent. Another criterion is that the gelator must be capable of self-organization to form a supramolecular network. This is necessary to immobilize the solvent with an infinite network of the gelator by self-assembly. Gelation processes with gelators also exhibit the characteristic features of gelation described above.[89,90]

6.3 Gelation and Vitrification. Gelation and vitrification (i.e., formation of a glass) are intriguing issues in polymer physics, which involve divergence of connectivity and freezing-in of dynamics, respectively. In the case of the former, chain connectivity diverges at the gelation point, and polymer chains are topologically frozen-in.[91] However, local chain motion is still allowed even after the gelation point. On the other hand, vitrification means a freezing-in process of the dynamics and is mainly attained by lowering the temperature or an increase in the population of the glass forming particles.

Vitrification has long been one of the central issues of soft condensed matter physics because of complexity of gel formation and scientific interests in glass transitions.[92] In many cases, glass transitions are discussed with respect to temperature. Here, on the other hand, we introduce a system undergoing vitrification with polymerization time for comparison between gelation and vitrification. The glass transition has been investigated by various techniques, such as viscoelasticity,[93] dielectrics, and thermal properties. Pioneering work on vitrification

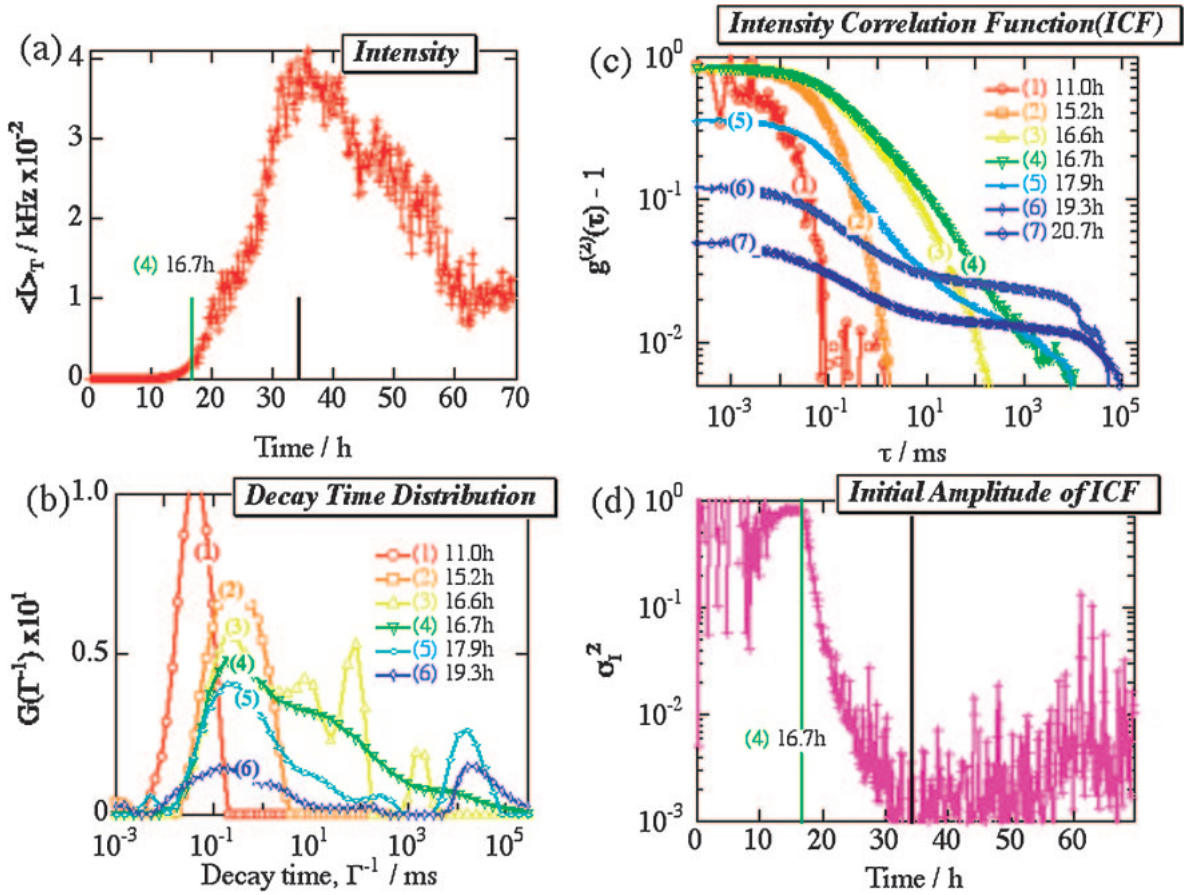

Fig. 23. Four methods to determine the gelation threshold: (a) steep intensity rise, (b) a power-law behavior in $g^{(2)}(q,\tau)-1$, (c) broadening of $G(\Gamma^{-1})$, and (d) suppression of the initial amplitude, σ_I^2 [Reproduced with permission from *Bull. Chem. Soc. Jpn.* **2002**, *75*, 641, Copyright permission: Chemical Society of Japan] (Fig. 12).

was carried out by Enns and Gillham, who proposed a time-temperature-transformation cure diagram for isothermal curing process of an amine-cured epoxy resin.[94] They predicted an "S"-shape TTT curve diagram and verified it by dynamical mechanical measurements. However, very few researchers discuss glass transitions from the viewpoint of chain connectivity.

Here, more ideal systems are discussed to answer the above questions, i.e., the bulk polymerization of styrene (St) and divinylbenzene (DVB). Both are one-component systems, but differ in their connectivity. St monomers only undergo linear extension, i.e., formation of linear polymer chains. The glass transition temperature (T_g) of polystyrene (PSt) is around 100 °C. Hence, vitrification may be observed during polymerization if the polymerization is carried out at a temperature below 100 °C. In the case of DVB, on the other hand, each monomer is capable of branching. Therefore, gelation as well as vitrification is expected during polymerization of DVB. In order to clarify the difference in the dynamics of polymer chains in the course of vitrification and gelation, TRDLS was carried out. As shown in Fig. 24a, the polymerization of St monomers exhibits two relaxation modes, i.e., collective diffusion and long relaxation of polymer chains in concentrated solutions. As the polymerization proceeds, the contribution from the collective diffusion mode diminishes. Finally, the system reaches the point where nonergodicity appears which is characterized by vigorous fluctuations in $\langle I\rangle_T$ and suppression of σ_I^2, which is followed by vitrification. On the other hand, systems capable of cross-linking (Figs. 24b and 24c) show a distinct gelation threshold, which is characterized by a power-law behavior in ICF (shown by the solid line) and the appearance of nonergodicity. In other words, gelation and vitrification can be clearly distinguished by TRDLS. In the case of the systems containing DVB, gelation is followed by vitrification, and the dynamics becomes similar to that of linear chains at the late stage of polymerization.

6.4 Universality and Specificity of Gelation Mechanism. The characteristic features in gelation threshold addressed in Section **6.1** were examined in many systems. Figure 25 shows a comparison of $g^{(2)}(\tau)$s across sol-to-gel-transition for three different systems: (a) PNIPA hydrogels having various NIPA concentrations,[81] (b) a gelatin gel during cooling process,[82] and (c) bulk-polymerization process of divinylbenzene (DVB).[95] All of them show a power-law behavior at the gelation threshold (marked in red), while the behavior after gelation depends on the system. PNIPA gels have only one relaxation mode, i.e., gel mode (or collective diffusion mode). The gelatin gel has a stretched exponential in addition to a gel mode. DVB reaches a sol–gel transition, which is followed by flattening of $g^{(2)}(\tau)$s, indicating vitrification. The lines in the figures represent curve fits with Eq. 29 or 41.

Table 2 summarizes the universality and specificity of gelation mechanisms of various types of gel which have been in-

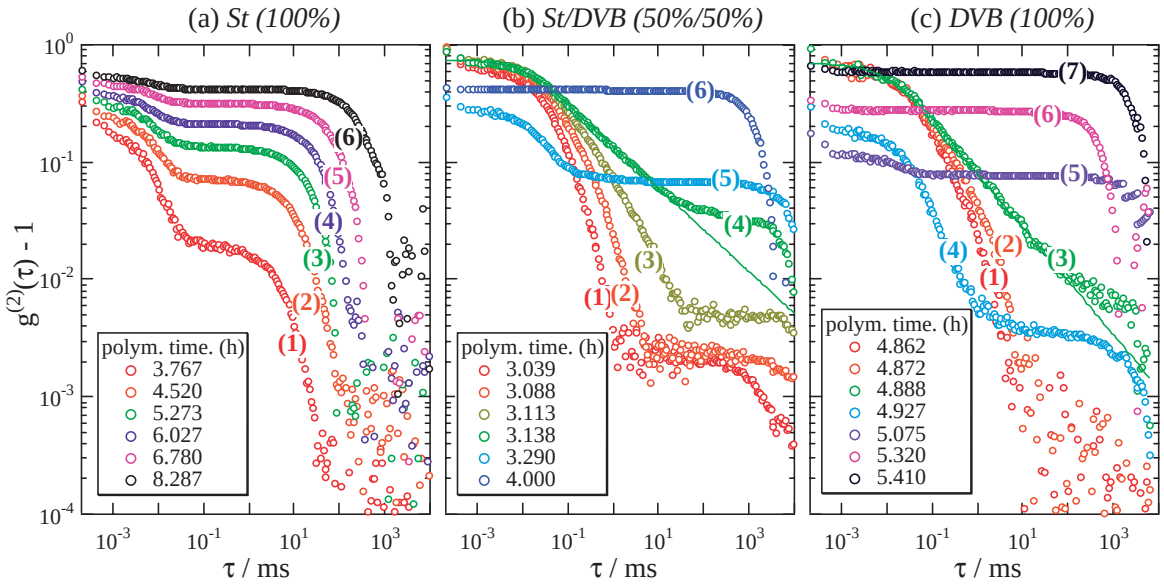

Fig. 24. Time-resolved dynamic light scattering (TRDLS) of bulk polymerization/cross-linking of (a) styrene (St), (b) a 50/50 mixture of styrene and divinylbenzene (St/DVB), and (c) DVB [Reproduced with permission from *Polymer* **2005**, *46*, 2381, Copyright permission: Elsevier] (Fig. 2).

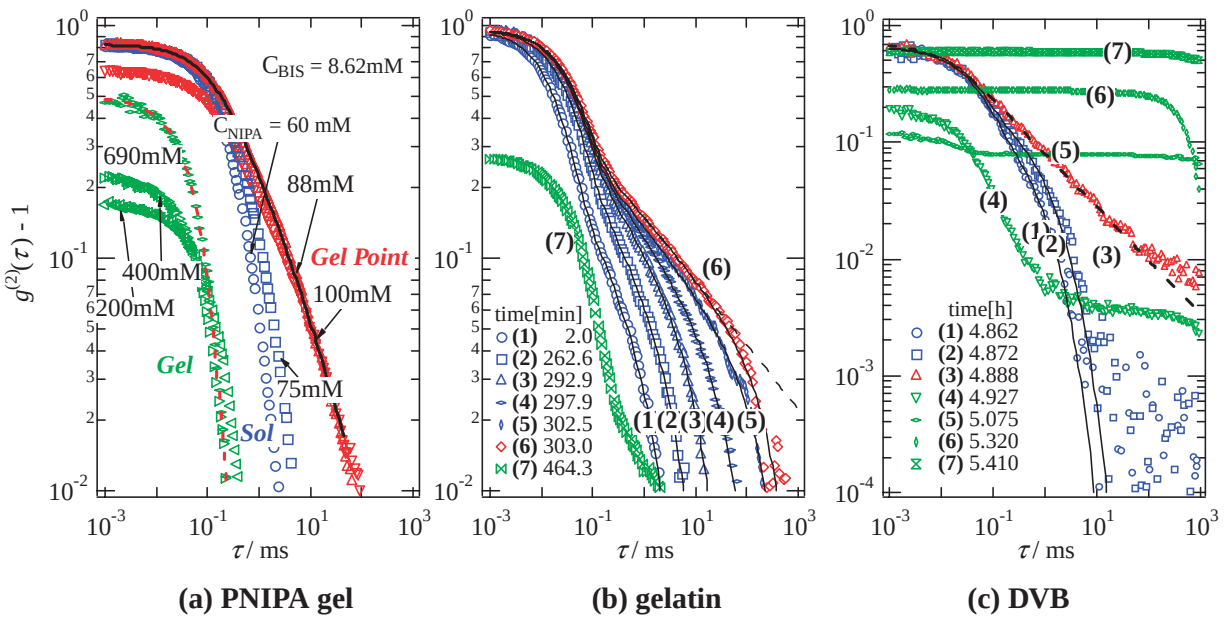

Fig. 25. Comparison of $g^{(2)}(q, \tau)$s across a sol-to-gel transition. (a) PNIPA hydrogels having various NIPA concentrations, (b) a gelatin gel during cooling process, (c) bulk-polymerization process of divinylbenzene (DVB).

vestigated so far: (a) chemical gels, (b) hybrid gels consisting of inorganic silica and organic polymer gels,[96,97] and polymer-clay nanocomposite gel,[98] (c) physical gels (PVA/CR,[66,99] β-lactoglobulin,[100] gelatin,[82,101] κ-carrageenan,[102] block copolymers[103]) and (d) gelators (aminoic acids,[89] salt complex[104]). It is essential to have (1) an increase in scattering intensity and (2) power-law behavior at gelation threshold, t_{gel}. However, the behavior in time-correlation function after gelation threshold seems to depend on the system. Roughly speaking, the behavior is classified as (a) exponential behavior, (b) stretched-exponential behavior, and (c) "frozen" behavior. The frozen behavior means a flattening of $g^{(2)}(\tau)$. It is concluded that all systems have common gelation features of gelation, while having specific differences. The former is the universality of gels as a bond-correlating system (a physical aspect). It includes an intensity increase (and an appearance of speckles) and a power-law behavior. On the other hand, the latter comes from the chemistry of the gel, such as gelation mechanism, chemical structure, functional groups, etc. (chemical aspect).

7. Hyper Gels and Future Direction

Recently, novel types of gels have been developed, such as slide-ring gel,[105] nanocomposite gel,[106] and double network gels.[107] Slide-ring gels were designed by completely different

Table 2. Universality and Specificity of Gelation Mechanism

	Intensity rise	Power law	
		$t \approx t_{gel}$	$t \gg t_{gel}$
(a) Chemical gel			
PNIPA	○	○	exp
PAAm	○	○	exp
TMOS	○	○	str.ex.
PSt/DVB	○	○	frozen
(b) Hybrid			
PNIPA/silica	○	○	str.ex.
PNIPA/clay	○	○	str.ex.
(c) Physical gel			
PVA/Congo	○	○	str.ex.
β-Lactoglobulin	○	○	str.ex.
Gelatin	○	○	str.ex.
κ-Carrageenan	○	○	str.ex.
Block copolymer	○	○	frozen
(d) Gelator			
Aminoic acid	○	○	frozen
Salt complex	○	○	frozen

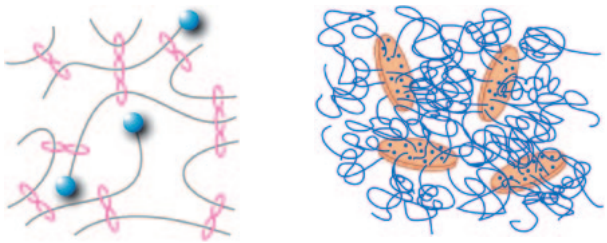

(a) "slide–ring" gel **(b) "nanocomposite" gel**

Fig. 26. Schematic illustration showing the network structure of hyper gels. (a) Slide-ring gel and (b) nanocomposite gel [Reproduced with permission from *Macromolecules* **2004**, *37*, 6177, and **2005**, *38*, 10772, Copyright permission: American Chemical Society] (Figs. 1 and 7).

concepts, i.e., "mobile" cross-links, which has changed the paradigm of cross-linking.[108] It was only in theorists' dreams that chains would be tied together by "slip-link" pulleys to model entanglements[109] and that elasticity of gels would be a consequence of their topology only.[42,110] This dream seemed dead from lack of implementation. Okumura and Ito were able to prepare of slide-ring gels by cross-linking polyrotaxane consisting of poly(ethylene glycol) (PEG) and cyclodextrin (CD) as shown in Fig. 26a.[111] CD molecules are able to slide along PEG chains. The sliding motion was verified by DLS,[112] and it was determined by using SANS to have only a small amount of inhomogeneities.[113]

Haraguchi and Takeshita developed nanocomposite gels, to which we will refer as NC gels, made of inorganic clay and polymer chains as schematically shown in Fig. 26b.[106] The clay is a thin disc that is 1 nm thick and 30 nm in diameter.[106] The gels consist of PNIPA and synthetic clay, laponite, and water. The NC gels have extraordinarily high mechanical properties, such as high elongation (greater than 10 times), high ultimate strength (of the order of 100 kPa), high transparency (structural homogeneity), large swelling/deswelling ratios, and high deswelling rates.[114,115] The origin of the high mechanical properties as well as gelation mechanism was investigated in terms of viscosity and turbidity measurements during gelation process and by X-ray diffraction on dried gels.[116] They reported that clay platelets are covered with NIPA monomers upon mixing. After polymerization is initiated, chain propagation takes place for monomers on a clay platelet by radical polymerization and ends with a monomer on the same or a neighboring platelet. Some of the chains may be terminated without reaching the surface of a clay platelet. The former becomes a looping or bridging chain and the latter does a dangling chain. Thus, a polymer network is formed with clay platelets as "plane" cross-linkers. The bottom line is that monomers with an amide group has to be used and polymerization has to be conducted in the presence of clay platelets in order to make strong contact between the network chains and cross-linkers.[117]

8. Concluding Remarks

Recent advances in the investigation of structure and dynamics of polymer gels are reviewed from the viewpoint of inhomogeneities. DLS and TRDLS are mainly used for elucidation of gel inhomogeneities and for decomposition of the two concentration fluctuations, i.e., thermal fluctuations and frozen inhomogeneities. Even in thermoreversible physical gels, significant degrees of inhomogeneities were found. The presence of inhomogeneities is characteristic of gels, and their formation is used to detect the gelation threshold.

A method to decompose the two concentration fluctuations is reviewed and is applied to various kinds of gels. It is clearly demonstrated that the preparation conditions affect both dynamic and static inhomogeneities, while the observation conditions affects only dynamic fluctuations. These findings provide useful information for application of gels. The universality and specificity of polymer gels are also addressed on the basis of a large number of DLS experiments for various types of gels. The universality includes speckles in light scattering intensity and power-law behavior in time-correlation functions. The specificity depends on the chemical structure and architecture of the gel and governs the physical properties of the gel.

Novel types of gels prepared based on very different concepts seem to open a new generation of functional/high performance gels. I would like to end this review by stating that the "fusion of the universality of physics and the particularity of chemistry" is a way of understanding of the complexity of gels.

Most of the work described in this article was carried out at the Department of Polymer Science and Engineering, Kyoto Institute of Technology, during the period of 1994 to 2000. The author is much indebted to his former students and his colleagues.

References

1 O. Wichterle, D. Lim, *Nature* **1960**, *185*, 117.
2 W. H. Stockmayer, *J. Chem. Phys.* **1943**, *11*, 45.
3 P. J. Flory, J. Rehner, Jr., *J. Chem. Phys.* **1943**, *11*, 521.
4 P. J. Flory, *Principles in Polymer Chemistry*, Cornell Univ., Ithaca, **1953**.
5 Y. Hirokawa, T. Tanaka, *J. Chem. Phys.* **1984**, *81*, 6379.

6 H. G. Schild, *Prog. Polym. Sci.* **1992**, *17*, 163.
7 M. Shibayama, *Macromol. Chem. Phys.* **1998**, *199*, 1.
8 S. Hirotsu, Y. Hirokawa, T. Tanaka, *J. Chem. Phys.* **1987**, *87*, 1392.
9 T. Tanaka, L. O. Hocker, G. B. Benedek, *J. Chem. Phys.* **1973**, *59*, 5151.
10 D. Stauffer, *J. Chem. Soc., Faraday Trans. 2* **1976**, *72*, 1354.
11 D. Stauffer, *Phys. Rep.* **1979**, *54*, 1.
12 D. Stauffer, *Introduction to Percolation Theory*, Taylor & Francis, London, **1985**.
13 T. Tanaka, *Polymer* **1979**, *20*, 1404.
14 T. Tanaka, *Sci. Am.* **1981**, *244*, 110.
15 M. Shibayama, T. Tanaka, *Adv. Polym. Sci.* **1993**, *109*, 1.
16 K. Dusek, D. Patterson, *J. Polym. Sci.* **1969**, *6*, 1209.
17 K. Dusek, *Responsive Gels: Volume Transitions I*, Springer-Verlag, Berlin, **1993**, Vol. 109.
18 K. Dusek, *Responsive Gels: Volume Transitions II*, Springer-Verlag, Berlin, **1993**, Vol. 110.
19 M. Annaka, T. Tanaka, *Nature* **1992**, *355*, 430.
20 S. Panyukov, Y. Rabin, *Phys. Rep.* **1996**, *269*, 1.
21 R. T. Deam, S. F. Edwards, *Philos. Trans. R. Soc. London, Ser. A* **1976**, *280*, 317.
22 M. Shibayama, T. Norisuye, *Bull. Chem. Soc. Jpn.* **2002**, *75*, 641.
23 F. Ikkai, M. Shibayama, *J. Polym. Sci., Part B: Polym. Phys.* **2005**, *43*, 617.
24 P. N. Pusey, W. van Megen, *Physica A* **1989**, *157*, 705.
25 W. van Megen, S. M. Underwood, P. N. Pusey, *Phys. Rev. Lett.* **1991**, *67*, 1586.
26 J. Z. Xue, D. J. Pine, S. T. Milner, X. L. Wu, P. M. Chaikin, *Phys. Rev. A* **1992**, *46*, 6550.
27 L. E. Reichl, *A Modern Course in Statistical Physics*, University of Texas, Austin, **1980**.
28 S. Mallam, F. Horkay, A. M. Hecht, E. Geissler, *Macromolecules* **1989**, *22*, 3356.
29 E. Mendes, F. Schosseler, F. Isel, F. Boue, J. Bastide, S. J. Candau, *Europhys. Lett.* **1995**, *32*, 273.
30 M. Shibayama, F. Ikkai, Y. Shiwa, Y. Rabin, *J. Chem. Phys.* **1997**, *107*, 5227.
31 M. Shibayama, K. Kawakubo, F. Ikkai, M. Imai, *Macromolecules* **1998**, *31*, 2586.
32 M. Shibayama, T. Norisuye, F. Ikkai, *J. Phys. Soc. Jpn.* **2001**, *70*, Suppl. A, 306.
33 S. Takata, T. Norisuye, M. Shibayama, *Macromolecules* **2002**, *35*, 4779.
34 T. Norisuye, N. Masui, Y. Kida, M. Shibayama, D. Ikuta, E. Kokufuta, S. Ito, S. Panyukov, *Polymer* **2002**, *43*, 5289.
35 M. Shibayama, in *Structure and Properties of Multi-Phase Polymeric Materials*, ed. by T. Araki, Q. Tran-Cong, M. Shibayama, Marcel Dekker, New York, **1998**, Vol. 6, pp. 195–231.
36 M. J. Orkisz, in *Physics*, Massachusetts Institute of Technology, Cambridge, **1994**, Vol. Ph.D.
37 J. C. Dainty, *Laser Speckle and Related Phenomena*, Springer-Verlag, Berlin, **1975**.
38 M. Born, E. Wolf, *Principles of Optics*, Pergamon Press, Oxford, **1975**.
39 A. F. J. Siegert, *MIT Radiat. Rep.* **1943**, 465.
40 L. D. Landau, E. M. Lifshitz, *Nauka: SSSR*, **1965**.
41 T. Tanaka, D. J. Fillmore, *J. Chem. Phys.* **1979**, *70*, 1214.
42 P. G. de Gennes, *Scaling Concepts in Polymer Physics*, Cornell University, Ithaca, **1979**.
43 T. Tanaka, in *Dynamic Light Scattering*, ed. by R. Pecora, Plenum Publishing, New York, **1985**, pp. 347–362.
44 J. G. H. Joosten, J. L. McCarthy, P. N. Pusey, *Macromolecules* **1991**, *24*, 6690.
45 M. Shibayama, T. Norisuye, S. Nomura, *Macromolecules* **1996**, *29*, 8746.
46 M. Shibayama, Y. Fujikawa, S. Nomura, *Macromolecules* **1996**, *29*, 6535.
47 M. Shibayama, S. Takata, T. Norisuye, *Physica A* **1998**, *249*, 245.
48 H. Furukawa, S. Hirotsu, *J. Phys. Soc. Jpn.* **2002**, *71*, 2873.
49 T. Norisuye, Q. Tran-Cong-Miyata, M. Shibayama, *Macromolecules* **2004**, *37*, 2944.
50 S. Takata, T. Norisuye, M. Shibayama, *Macromolecules* **1999**, *32*, 3989.
51 J. A. Zurimendi, S. J. Guerrero, V. Leon, *Polymer* **1984**, *25*, 1314.
52 F. Ikkai, M. Shibayama, *Phys. Rev. E* **1997**, *56*, R51.
53 M. Shibayama, F. Ikkai, S. Inamoto, S. Nomura, C. C. Han, *J. Chem. Phys.* **1996**, *105*, 4358.
54 M. Shibayama, Y. Shirotani, Y. Shiwa, *J. Chem. Phys.* **2000**, *112*, 442.
55 H. Furukawa, K. Horie, R. Nozaki, M. Okada, *Phys. Rev. E* **2003**, *68*, 031406.
56 J. Bastide, L. Leibler, *Macromolecules* **1988**, *21*, 2647.
57 C. Nakamoto, T. Motonaga, M. Shibayama, *Macromolecules* **2000**, *34*, 911.
58 M. Shibayama, K. Isono, S. Okabe, T. Karino, M. Nagao, *Macromolecules* **2004**, *37*, 2909.
59 T. Norisuye, Y. Kida, N. Masui, Q. Tran-Cong-Miyata, Y. Maekawa, M. Yoshida, M. Shibayama, *Macromolecules* **2003**, *36*, 6202.
60 A. Y. Grosberg, S. K. Nechaev, *Macromolecules* **1991**, *24*, 2789.
61 Y. A. Kuznetsov, E. G. Thimoshenko, K. A. Dawson, *J. Chem. Phys.* **1996**, *104*, 3338.
62 Y. A. Kuznetsov, E. G. Timoshenko, K. A. Dawson, *J. Chem. Phys.* **1995**, *103*, 4807.
63 R. Yoshida, K. Uchida, Y. Kaneko, K. Sakai, A. Kikuchi, Y. Sakurai, T. Okano, *Nature* **1995**, *374*, 240.
64 S. Takata, K. Suzuki, M. Shibayama, T. Norisuye, *Polymer* **2002**, *43*, 3101.
65 M. Shibayama, K. Nagai, *Macromolecules* **1999**, *32*, 7461.
66 F. Ikkai, M. Shibayama, *Phys. Rev. Lett.* **1999**, *82*, 4946.
67 M. Shibayama, F. Ikkai, R. Moriwaki, S. Nomura, *Macromolecules* **1994**, *27*, 1738.
68 M. Shibayama, F. Ikkai, S. Nomura, *Macromolecules* **1994**, *27*, 6383.
69 E. Z. Cassasa, A. M. Sarquis, C. H. Van Dyke, *J. Chem. Educ.* **1986**, *63*, 57.
70 M. Shibayama, M. Sato, Y. Kimura, H. Fujiwara, S. Nomura, *Polymer* **1988**, *29*, 336.
71 M. Shibayama, H. Yoshizawa, H. Kurokawa, H. Fujiwara, S. Nomura, *Polymer* **1988**, *29*, 2066.
72 M. Shibayama, T. Takeuchi, S. Nomura, *Macromolecules* **1994**, *27*, 5350.
73 M. Shibayama, M. Uesaka, Y. Shiwa, *J. Chem. Phys.* **1996**, *105*, 4350.
74 M. Shibayama, R. Moriwaki, F. Ikkai, S. Nomura, *Polymer* **1994**, *26*, 5716.
75 K. te Nijenhuis, *Adv. Polym. Sci.* **1997**, *130*, 1.

76 J. S. Hwang, H. Z. Cummins, *J. Chem. Phys.* **1983**, *79*, 5188.
77 E. J. Amis, P. A. Janmey, J. D. Ferry, H. Yu, *Macromolecules* **1983**, *16*, 441.
78 T. Herning, M. Djabourov, J. Leblond, G. Takerkart, *Polymer* **1991**, *32*, 3211.
79 I. Pezron, M. Djabourov, J. Leblond, *Polymer* **1991**, *32*, 3201.
80 T. Norisuye, M. Shibayama, S. Nomura, *Polymer* **1998**, *39*, 2769.
81 M. Takeda, T. Norisuye, M. Shibayama, *Macromolecules* **2000**, *33*, 2909.
82 M. Okamoto, T. Norisuye, M. Shibayama, *Macromolecules* **2001**, *34*, 8496.
83 J. E. Martin, J. Wilcoxon, *Phys. Rev. Lett.* **1988**, *61*, 373.
84 M. Adam, D. Lairez, in *Physical Properties of Polymeric Gels*, ed. by J. P. Cohen Addad, John Wiley & Sons, New York, **1996**, p. 87.
85 M. Muthukumar, H. H. Winter, *Macromolecules* **1986**, *19*, 1284.
86 M. Shibayama, T. Norisuye, *AIP Conf. Proc.* **1999**, *469*, 85.
87 K. Hanabusa, R. Tanaka, M. Suzuki, M. Kimura, H. Shirai, *Adv. Mater.* **1997**, *9*, 1095.
88 P. Terech, R. G. Weiss, *Chem. Rev.* **1997**, *97*, 3133.
89 S. Okabe, K. Andoh, K. Hanabusa, M. Shibayama, *J. Polym. Sci., Part B: Polym. Phys.* **2004**, *42*, 1841.
90 S. Okabe, K. Hanabusa, M. Shibayama, *J. Polym. Sci., Part B: Polym. Phys.* **2005**, *43*, 3567.
91 J. M. Guenet, *Thermoreversible Gelation of Polymers and Biopolymers*, Academic Press, NY, **1992**.
92 E. Donth, *The Glass Transition*, Springer, Berlin, **2001**.
93 J. D. Ferry, *Viscoelastic Properties of Polymers*, 3rd. ed., Wiley, New York, **1980**.
94 J. B. Enns, L. K. Gillham, *J. Appl. Polym. Sci.* **1983**, *28*, 2567.
95 M. Shibayama, S. Ozeki, T. Norisuye, *Polymer* **2005**, *46*, 2381.
96 T. Norisuye, M. Shibayama, R. Tamaki, Y. Chujo, *Macromolecules* **1999**, *32*, 1528.
97 T. Norisuye, M. Inoue, M. Shibayama, R. Tamaki, Y. Chujo, *Macromolecules* **2000**, *33*, 900.
98 M. Shibayama, J. Suda, T. Karino, S. Okabe, T. Takehisa, K. Haraguchi, *Macromolecules* **2004**, *37*, 9606.
99 M. Tsujimoto, M. Shibayama, *Macromolecules* **2002**, *35*, 1342.
100 S. Takata, T. Norisuye, N. Tanaka, M. Shibayama, *Macromolecules* **2000**, *33*, 5470.
101 M. Shibayama, M. Okamoto, *J. Chem. Phys.* **2001**, *115*, 4285.
102 L. Abad, I. R. Nasimova, L. Relleve, C. T. Aranilla, A. M. Dela Rosa, M. Shibayama, *Int. J. Biol. Macromol.* **2004**, *34*, 81.
103 S. Okabe, S. Sugihara, S. Aoshima, M. Shibayama, *Macromolecules* **2003**, *36*, 4099.
104 P. Dastidar, S. Okabe, K. Nakano, K. Iida, M. Miyata, N. Thonai, M. Shibayama, *Chem. Mater.* **2005**, *17*, 741.
105 Y. Okumura, K. Ito, *Adv. Mater.* **2001**, *13*, 485.
106 K. Haraguchi, T. Takeshita, *Adv. Mater.* **2002**, *14*, 1120.
107 J. P. Gong, Y. Katsuyama, T. Kurokawa, Y. Osada, *Adv. Mater.* **2003**, *15*, 1115.
108 S. Granick, M. Rubinstein, *Nat. Mater.* **2004**, *3*, 586.
109 R. C. Ball, M. Doi, S. F. Edwards, *Polymer* **1981**, *22*, 1010.
110 P. G. de Gennes, *Physica A* **1999**, *271*, 231.
111 T. Karino, Y. Okumura, K. Ito, M. Shibayama, *Macromolecules* **2004**, *37*, 6177.
112 C. Zhao, Y. Domon, Y. Okumura, S. Okabe, M. Shibayama, K. Ito, *J. Phys. Condens. Matter* **2005**, *17*, S2841.
113 T. Karino, Y. Okumura, C. Zhao, T. Kataoka, K. Ito, M. Shibayama, *Macromolecules* **2005**, *38*, 6161.
114 K. Haraguchi, T. Takeshita, S. Fan, *Macromolecules* **2002**, *35*, 10162.
115 K. Haraguchi, R. Farnworth, A. Ohbayashi, T. Takehisa, *Macromolecules* **2003**, *36*, 5732.
116 K. Haraguchi, H.-J. Li, K. Matsuda, T. Takehisa, E. Elliot, *Macromolecules* **2005**, *38*, 3482.
117 M. Shibayama, T. Karino, S. Miyazaki, T. Takehisa, K. Haraguchi, *Macromolecules* **2005**, *38*, 10772.

Mitsuhiro Shibayama was born in 1954. He graduated from the Department of Polymer Chemistry, Faculty of Engineering, Kyoto University in 1977. He received a Doctor-of-Engineering degree from Kyoto University in 1983. After serving as a fellow of the Japan Society for Promotion of Science and as a research associate at the University of Massachusetts at Amherst, he joined the Department of Polymer Science, Kyoto Institute of Technology in 1984. He was promoted to an associate professor in 1988 and to a professor in 1997. In 1991, he spent a year at Physics Department, Massachusetts Institute of Technology. In 2000, he moved to Neutron Scattering Laboratory, Institute for Solid State Physics, the University of Tokyo. His research interest covers structure investigation and dynamics of multi-component polymeric systems with various scattering techniques, such as small-angle neutron scattering and dynamic light scattering. He has received the Sakurada Takeshi Memorial Award (Japan Fiber Society, 1991) and the Wiley Science Award (the Society of Polymer Science, Japan, 2000).